SCIENTIFIC REPORTS

OPEN

SUBJECT AREAS:
CHEMOTHERAPY
BREAST CANCER

Received
16 July 2014

Accepted
29 October 2014

Published
18 November 2014

Correspondence and requests for materials should be addressed to H.H. (hiromi_hiyoshi@tara.tsukuba.ac.jp)

2-(4-Hydroxy-3-methoxyphenyl)-benzothiazole suppresses tumor progression and metastatic potential of breast cancer cells by inducing ubiquitin ligase CHIP

Hiromi Hiyoshi[1,2], Natsuka Goto[1], Mai Tsuchiya[1], Keisuke Iida[3], Yuka Nakajima[1,2], Naoya Hirata[4], Yasunari Kanda[4], Kazuo Nagasawa[3] & Junn Yanagisawa[1,2]

[1]Graduate School of Life and Environmental Sciences, University of Tsukuba, 1-1-1 Tennodai, Tsukuba 305-8577, Japan, [2]Center for Tsukuba Advanced Research Alliance, University of Tsukuba, 1-1-1 Tennodai, Tsukuba 305-8577, Japan, [3]Faculty of Technology, Tokyo University of Agriculture and Technology-TUAT, 2-24-16 Naka-cho, Koganei-shi, Tokyo 185-0031, Japan, [4]Division of Pharmacology, National Institute of Health Sciences, 1-18-1, Kamiyoga, Setagaya-ku 158-8501, Japan.

Breast cancer is the most common malignancy among women and has poor survival and high recurrence rates for aggressive metastatic disease. Notably, triple-negative breast cancer (TNBC) is a highly aggressive cancer and there is no preferred agent for TNBC therapy. In this study, we show that a novel agent, 2-(4-hydroxy-3-methoxyphenyl)-benzothiazole (YL-109), has ability to inhibit breast cancer cell growth and invasiveness *in vitro* and *in vivo*. In addition, YL-109 repressed the sphere-forming ability and the expression of stem cell markers in MDA-MB-231 mammosphere cultures. YL-109 increased the expression of carboxyl terminus of Hsp70-interacting protein (CHIP), which suppresses tumorigenic and metastatic potential of breast cancer cells by inhibiting the oncogenic pathway. YL-109 induced *CHIP* transcription because of the recruitment of the aryl hydrocarbon receptor (AhR) to upstream of *CHIP* gene in MDA-MB-231 cells. Consistently, the antitumor effects of YL-109 were depressed by *CHIP* or *AhR* knockdown in MDA-MB-231 cells. Taken together, our findings indicate that a novel agent YL-109 inhibits cell growth and metastatic potential by inducing CHIP expression through AhR signaling and reduces cancer stem cell properties in MDA-MB-231 cells. It suggests that YL-109 is a potential candidate for breast cancer therapy.

Breast cancer is the major cause of cancer death among women worldwide. Triple-negative breast cancer (TNBC), which has been reported to represent approximately 15% of all breast cancers[1], is characterized by the absence of estrogen receptors (ERs), progesterone receptors (PRs), and human epidermal growth factor-2 (HER-2) expression[2]. TNBC is an aggressive cancer, characterized by rapid tumor growth, a high incidence of metastasis, an increased rate of distant recurrence, and a poor prognosis compared with other breast cancer subtypes[3]. Unlike ER/PR-positive or HER-2-overexpressing subtypes, the effective treatment options for TNBC are limited to cytotoxic therapies because of the lack of molecular targets. Moreover, TNBC cells show a profile that is similar to breast cancer stem cells, which have a strong resistance to chemotherapeutic drugs[4,5]. Therefore, new therapeutic options and strategies are required for TNBC therapy.

The carboxyl terminus of Hsp70-interacting protein (CHIP, also named STUB1) is a potential target for the treatment of TNBC. CHIP is a U-box-type ubiquitin E3 ligase that induces ubiquitylation and degradation of its substrates. These include several oncogenic proteins that suppress the tumorigenic and metastatic potential of breast cancer cells[6–8]. We previously reported that CHIP levels were much higher in MCF-7 cells, a non-aggressive cell line derived from human breast cancer cells, than in MDA-MB-231 cells, a highly aggressive cell line. Furthermore, CHIP levels are negatively correlated with the malignancy of human breast tumor tissues[9]. In addition, CHIP suppresses both tumor growth and metastasis in a nude mouse xenograft model. Thus, it has been suggested that the regulation of CHIP expression may represent a potential new clinical approach to TNBC therapy.

Aryl hydrocarbon receptor (AhR) has also recently emerged as a potential therapeutic target for breast cancer. The AhR is a basic helix-loop-helix transcription factor that was initially identified as a receptor for environmental toxins, such as dioxin[10]. Ligand binding to the receptor triggers formation of a heterodimeric nuclear AhR complex, which binds to dioxin response elements in target gene promoters to induce transcriptional activation[11]. Several studies have demonstrated that the AhR may be a potential drug target for several diseases, including endometrial, prostate, pancreatic, and ER-positive breast cancers[12–17]. In addition, the antitumor effects of compounds belonging to the 2-(4-amino-3-methylphenyl) benzothiazole group are mediated by AhR in ER-positive breast cancer cells[18–20]. Phortress, the lysine amide prodrug of 2-(4-amino-3-methylphenyl)-5-fluorobenzothiazole, has completed Phase I clinical evaluations[18,21]. In addition to 2-(4-aminophenyl) benzothiazoles, the relatively non-toxic selective AhR modulators (SAhRMs) are highly effective agents for inhibiting hormone-responsive breast cancer growth in animal models[17,22]. Although 2-(4-aminophenyl) benzothiazoles and SAhRMs are less effective against ER-negative breast cancer cells, AhR is also expressed in these cells[18,23,24]. Therefore, we hypothesized that ideal agents might exert the antitumor effects mediated by AhR signaling in both ER-positive and -negative breast cancer cells.

In this study, we demonstrated that the novel agent 2-(4-hydroxy-3-methoxyphenyl)-benzothiazole (YL-109) has ability to inhibit breast cancer progression in TNBC, MDA-MB-231 cells, and ER-positive breast cancer MCF-7 cells. In addition, YL-109 suppresses the proliferation and invasiveness of MDA-MB-231 cells, both *in vitro* and *in vivo*. Moreover, YL-109 suppresses the properties of breast cancer stem cells. Furthermore, we demonstrated that YL-109 increases *CHIP* expression by the recruitment of AhR to an upstream region of the gene. Consistent with these observations, CHIP or AhR knockdowns inhibit the suppressive effects of YL-109 on anchorage-independent growth and invasiveness. Taken together, our findings indicate that YL-109 is a novel antitumor agent that can induce CHIP expression through AhR signaling, and that it represents a promising candidate for a new therapeutic strategy against TNBC.

Results

YL-109 inhibits cell proliferation, motility, and invasiveness in breast cancer cells. It has been reported that 2-(4-aminophenyl)-benzothiazoles have anti-proliferative activity in MCF-7, ER-positive breast cancer cells[18–20]. Therefore, we investigated the effects of 2-(4-hydroxy-3-methoxyphenyl)-benzothiazole, YL-109 (Figure 1a) on cell proliferation in MCF-7 cells. YL-109 possesses characteristic hydroxyl group at C4, whereas 2-(4-aminophenyl)-benzothiazoles have the amino group at this position. YL-109 strongly inhibited cell proliferation of MCF-7 cells in a dose-dependent manner (IC_{50} = 85.8 nM) (Figure 1b and c). Surprisingly, YL-109 had an anti-proliferative effect in a dose-dependent manner (IC_{50} = 4.02 μM) on MDA-MB-231 cells, known as TNBC cells, unlike 2-(4-aminophenyl)-benzothiazoles (Figure 1b and c)[18]. We subsequently tested whether YL-109 inhibited anchorage-independent growth in poly-HEMA coated plates and colony formation in soft agar (Figure 1d and e). Under short-term detached conditions using poly-HEMA coated plate, YL-109 suppressed cell survival in MCF-7 cells, but not in MDA-MB-231 cells (Figure 1d). In contrast, YL-109 decreased the number of colonies in MDA-MB-231 cells under long-term detached conditions on soft agar (Figure 1e). Moreover, to examine the effects of YL-109 on the metastatic and invasive potential of MDA-MB-231 cells, we performed migration and invasion assays. In the migration assay, YL-109 reduced the ability of cells to migrate (Figure 1f). YL-109 also significantly decreased the number of cells that penetrated the Matrigel-coated membrane (Figure 1g). In addition, YL-109 inhibited cell proliferation and invasiveness of BT-20 cells, also known as TNBC cells (see Supplementary Fig. S1 online). These results suggest that YL-109 inhibits cell proliferation and suppresses the metastatic potential of breast cancer cells.

YL-109 inhibits both tumor growth and cancer metastasis of breast cancer cells *in vivo*. Using a nude mouse xenograft model, we investigated the effects of YL-109 *in vivo*. Mice treated with vehicle showed significantly enlarged tumors, whereas mice treated with YL-109 showed attenuated tumor growth using MCF-7 cells (Figure 2a). Interestingly, YL-109 also suppressed tumor growth in mice injected with MDA-MB-231 cells (Figure 2b). Next, to examine the effect of YL-109 against metastatic activity, we performed an *in vivo* lung metastasis assay using MDA-MB-231 cells. We discovered several metastatic tumors in the lungs of mice injected with MDA-MB-231 cells in the vehicle (Figure 2c). Compared with the vehicle control, YL-109 significantly reduced lung metastasis (Figure 2c). We also quantified lung metastasis using real-time RT-PCR, which confirmed our observations (Figure 2d). These results suggest that YL-109 suppresses tumor progression of breast cancer cells *in vivo*.

YL-109 suppresses breast cancer progression by inducing CHIP expression. We previously demonstrated that CHIP suppresses tumorigenesis and the metastatic cellular phenotypes of breast cancer cells both *in vitro* and *in vivo*[9]. It has also been indicated that CHIP expression is significantly associated with prognostic parameters in breast cancer patients[25]. Therefore, we examined whether YL-109 induced CHIP expression. We observed that YL-109 increased both CHIP mRNA and protein levels (Figure 3a and b). Next, to investigate whether the antitumor effects of YL-109 were mediated by CHIP, we performed colony formation and Matrigel invasion assay using siRNA for CHIP (Figure 3c–e). YL-109-induced inhibition of cell growth and invasive potential were decreased by CHIP knockdown (Figure 3d and e). These results demonstrate that YL-109 inhibits breast cancer progression by inducing CHIP expression.

YL-109 activates AhR signaling to induce CHIP expression. Previous studies indicated that 2-(4-aminophenyl)-benzothiazoles activate AhR and increase transcription of AhR target genes, such as *Cyp1a1*[18–20]. We observed that YL-109 induced *Cyp1a1* expression in MCF-7 and MDA-MB-231 cells (Figure 4a). To explore AhR participation in the mechanisms underlying the induction of CHIP by YL-109, we examined whether CHIP expression levels were affected by knocking down of AhR with siRNA (Figure 4b and c). We observed that YL-109-induced increases in *CHIP* mRNA were reduced by AhR knockdown (Figure 4c). We subsequently examined AhR recruitment to the promoter region in *CHIP* gene, which contains potential AhR response elements. Chromatin immunoprecipitation (ChIP) assay demonstrated that the interaction between AhR and the *CHIP* promoter is potentiated by YL-109 (Figure 4d). Our data suggest that YL-109 induces CHIP expression through recruitment of AhR to upstream of *CHIP* gene.

YL-109 exerts antitumor effects through AhR signaling. To examine whether AhR signaling mediated the inhibition of cell proliferation by YL-109, we performed MTT assay using the AhR antagonist α-naphtoflavone (α-NF) and siRNA against AhR (Figure 5a and b). Treatment with α-NF and knockdown of AhR expression abolished the inhibitory effect of YL-109 on cell proliferation of MCF-7 cells (Figure 5a and b). Moreover, YL-109-induced inhibition of colony formation and invasive potential were repressed by AhR knockdown (Figure 5c and d). Our data suggest that the antitumor effects of YL-109 are mediated by AhR signaling.

YL-109 reduces the property of cancer stem cells in breast cancer cells. Recently, we have shown that CHIP suppresses cancer stem cell properties in breast cancer cells[26]. Therefore, we evaluated whether

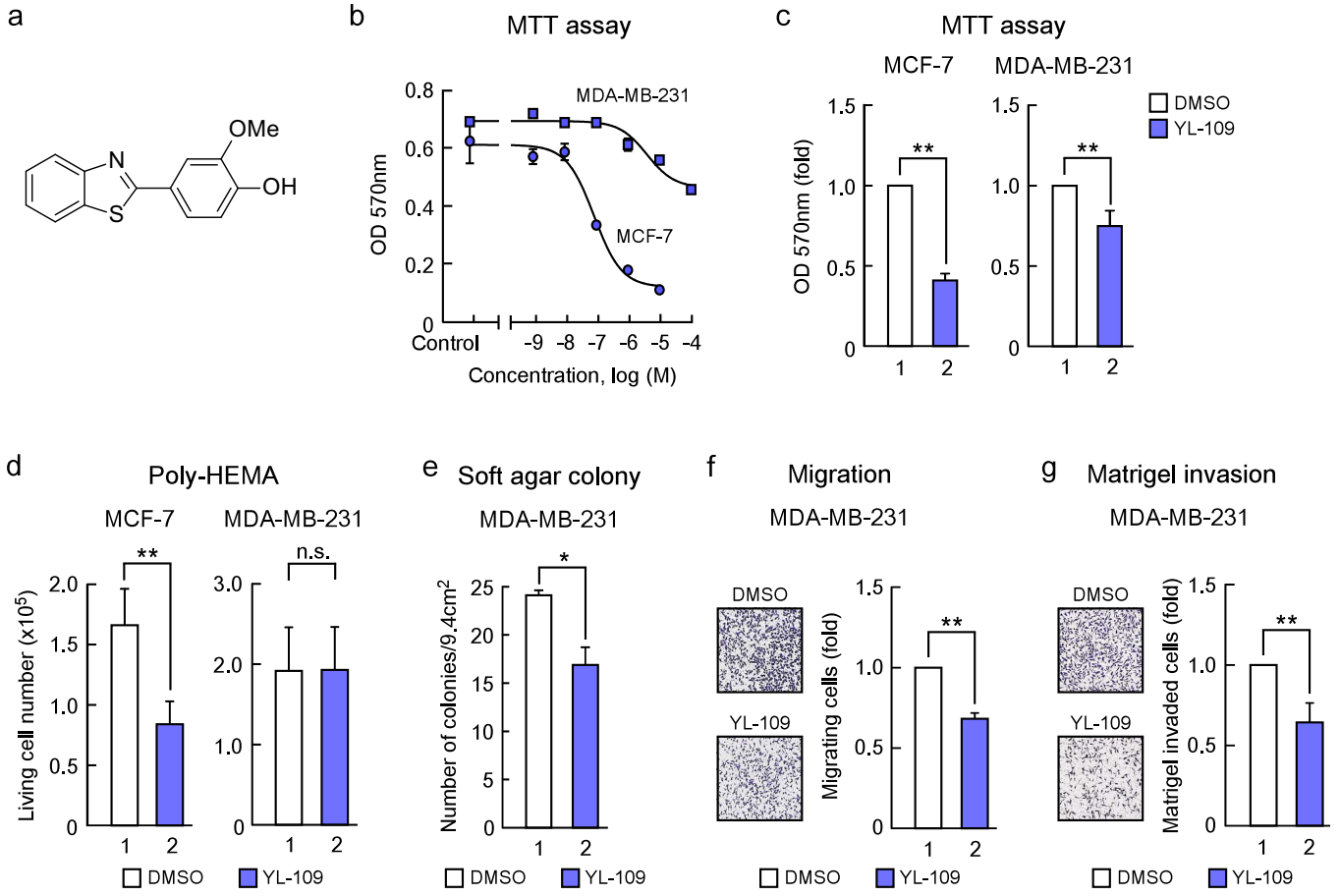

Figure 1 | Identification of a compound that inhibits cell proliferation, motility and invasiveness in breast cancer cells. (a) Structure of 2-(4-hydroxy-3-methoxyphenyl)-benzothiazole, YL-109. (b) Effects of YL-109 on cell proliferation in breast cancer cells. MCF-7 or MDA-MB-231 cells were cultured with the indicated concentration (shown as -logM) of YL-109. After 96 h, MTT assay was performed (MCF-7; IC_{50} = 85.8 nM, MDA-MB-231; IC_{50} = 4.02 μM). (c) Effects of YL-109 on anchorage-dependent cell growth in breast cancer cells. MCF-7 or MDA-MB-231 cells were cultured in media containing DMSO or YL-109 (1 μM) for 96 h. The cell viability was measured by MTT assays. (d and e) Effects of YL-109 on anchorage-independent cell growth in breast cancer cells. Cells were plated on poly-HEMA (d) or soft agar (e) coated plates in the absence or presence of YL-109 (1 μM). The viable cells were counted using Countess Automated Cell Counter (Invitrogen) (d). The colonies were examined under a microscope and colonies with a diameter of more than 100 μm were counted (e). (f and g) Effects of YL-109 on cell motility and invasiveness in MDA-MB-231 cells. MDA-MB-231 cells were seeded onto filters with an 8 μm pore size in uncoated (f, migration assay) or Matrigel matrix-coated (g, invasion assay) upper chambers in the absence or presence of YL-109 (1 μM). * indicates $p<0.05$ and ** indicates $p<0.01$ and n.s. indicates $p>0.05$ by student's T test vs. DMSO-treated cells.

YL-109 affects breast cancer stem cells. One property of cancer stem cells is their ability to form tumor spheres, denoted mammospheres in the case of breast cancer[27]. We observed that cells derived from the MDA-MB-231 cell line formed mammospheres, whereas YL-109 markedly inhibited mammosphere formation (Figure 6a). To confirm the effects of YL-109 on the population of cancer stem cells in MDA-MB-231 cells, we used flow cytometry with cancer stem cell marker ALDH. Consistent with the effects on mammosphere formation, YL-109 decreased ALDH-positive cell population (Figure 6b). In addition, YL-109 significantly decreased mRNA levels of *Klf-4* and Notch target gene *Hes1* in MDA-MB-231 mammosphere cultures (Figure 6c). Taken together, these results indicate that YL-109 inhibits the properties of breast cancer stem cells.

Discussion

In the present study, we revealed that the novel agent YL-109 has antitumor activity in TNBC cells. It was previously reported that 2-(4-aminophenyl)-benzothiazoles have anti-proliferative activity in ER-positive breast cancer cells, that is mediated by the AhR signaling pathway. AhR is expressed in breast cancer cells regardless of ER expression[23,24]. However, TNBC cells exhibit a poor response to benzothiazoles and SAhRMs because they do not activate AhR -signaling[18]. Consistent with previous reports on benzothiazole anti-tumor activity, YL-109 inhibited cell proliferation through AhR activation in ER-positive breast cancer cells. In addition, we observed that YL-109 could activate AhR signaling in MDA-MB-231 cells, which is necessary for YL-109 to exert antitumor effects in these cells. These results suggest that YL-109 inhibits breast cancer progression by AhR signaling activation in TNBC cells.

Our results also demonstrated that the YL-109-induced AhR signaling activation resulted in increased CHIP expression. We previously reported that CHIP suppresses tumor progression in human breast cancer by inhibiting oncogenic pathways[9]. In mice, tumor growth and metastasis were significantly inhibited by CHIP expression, whereas CHIP knockdowns in breast cancer cells resulted in rapid tumor growth and metastatic phenotypes. In this study, we observed that YL-109 treatment increased CHIP expression and CHIP knockdown inhibited the suppressive effects of YL-109 on both breast cancer cell growth and invasiveness. Moreover, YL-109 induced CHIP expression by recruiting AhR to an upstream region of the *CHIP* gene. We also found that the multiple AhR-responsive element sites exist in the promoter region of *CHIP*, which contain the core sequence 5′-GCGTG-3′. Taken together, these findings indicate

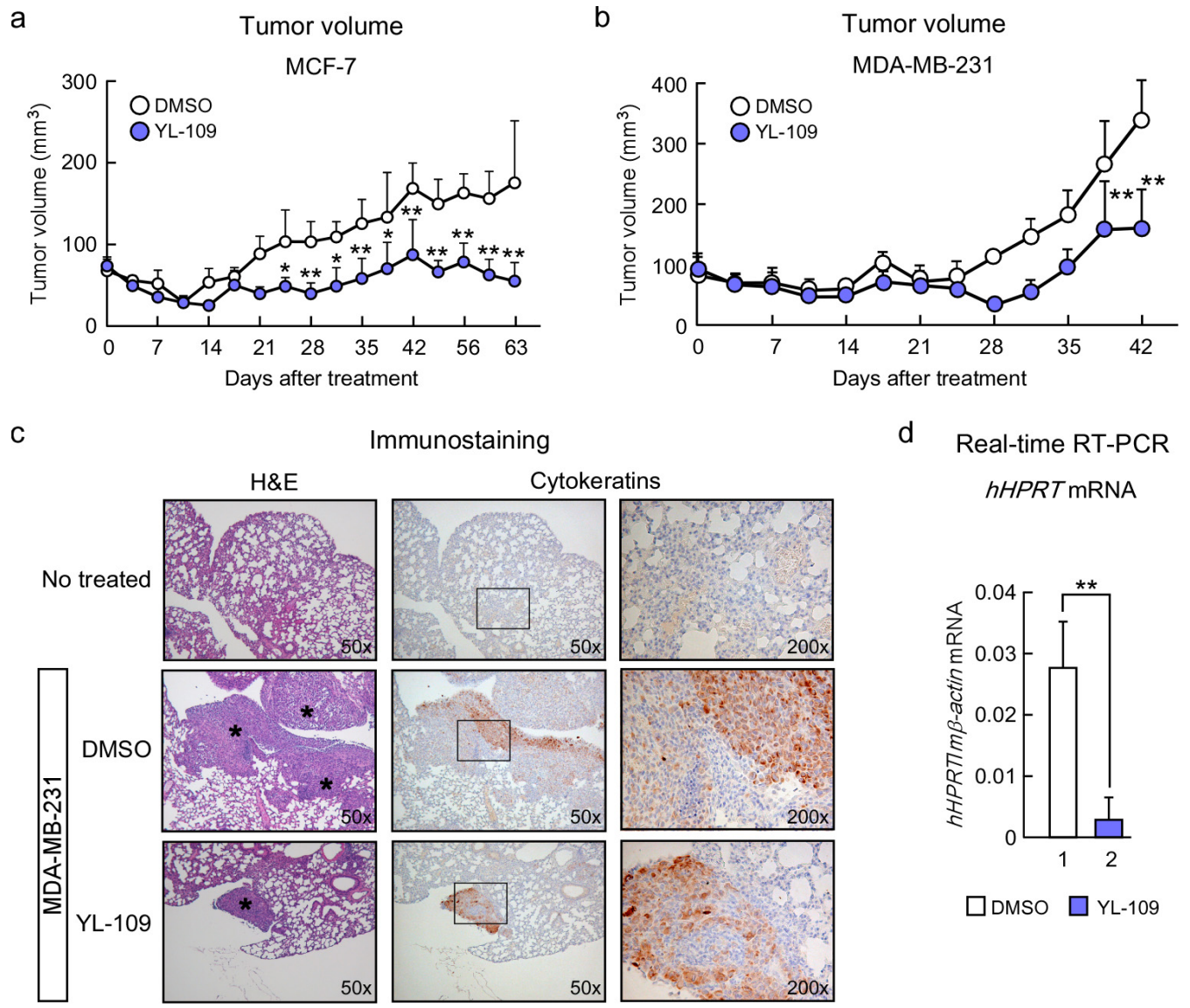

Figure 2 | **YL-109 suppresses both tumor growth and metastasis of breast cancer cells *in vivo*.** (a and b) Effects of YL-109 on tumor growth in a mouse xenograft model. Mice were treated with DMSO (vehicle) or YL-109 (15 mg/kg) for every 2 days. Tumor growth curves showed tumor volume in nude mice inoculated with MCF-7 (a) or MDA-MB-231 cells (b). Tumor growth was monitored twice each week. Bars represent mean + s.d. (n=3–6). * indicates $p<0.05$ and ** indicates $p<0.01$ by two-way ANOVA with Bonferroni's post hoc test. (c and d) Effects of YL-109 on tumor metastasis *in vivo*. MDA-MB-231 cells were injected into the tail veins of nude mice. Forty-two days after the injections, lungs were collected. Representative images of sections from lungs are shown (c). Left panels show the images of H&E staining (50x). Immunohistochemistry for human cytokeratins is shown in middle (50x) and right (200x) panels. Asterisks indicate metastatic tumor growth. The lung metastasis was quantified by real-time RT–PCR (d). Specific primers for human *HPRT* were used. * indicates $p<0.05$ and ** indicates $p<0.01$ by student's T test vs. DMSO-treated mice.

that YL-109 inhibits breast cancer progression by inducing CHIP expression through AhR signaling.

Our data demonstrated that YL-109 increased CHIP levels in MDA-MB-231 cells. We also observed that YL-109 inhibited anchorage-independent cell growth in soft agar as well as xenograft tumor growth, but not in poly-HEMA coated plates. For assays of *in vitro* cell growth, cells were detached and suspended, either in poly-HEMA coated plates for 24 h, or in soft agar for 3 weeks. In short-term growth experiments such as the poly-HEMA assay, we did not observe cell growth inhibition by YL-109, because YL-109-induced inhibition of cell growth presumably requires the elevation of CHIP levels. Consistent with this, in long-term growth experiments such as soft agar colony formation and xenograft tumor growth, YL-109 inhibited cell growth of TNBC cells. Furthermore, this effect was repressed by the knockdown of CHIP or AhR in TNBC cells.

In contrast, CHIP levels are considerably higher in MCF-7 cells than in MDA-MB-231 cells, and we observed that YL-109 did not affect CHIP expression in MCF-7 cells (data not shown). However, YL-109 was able to inhibit the growth of MCF-7 cells in both short-term and long-term growth experiments. These observations suggest that CHIP does not contribute to the effects of YL-109 on cell growth in ER-positive breast cancer cells.

Previous studies have reported that the inhibition of ER signaling can result from cross talk with the ligand-activated AhR. AhR ligands strongly suppress estrogen-induced responses in the rodent uterus, mammary tumors, and human breast cancer cells[28]. Treatment of ER-positive breast cancer cells with 2,3,7,8-tetrachlorodeibenzo-p-dioxin (TCDD) induces proteasome-dependent degradation of endogenous ERα[29]. In this study, we demonstrated that YL-109 inhibits cell proliferation through the AhR signaling pathway in MCF-7

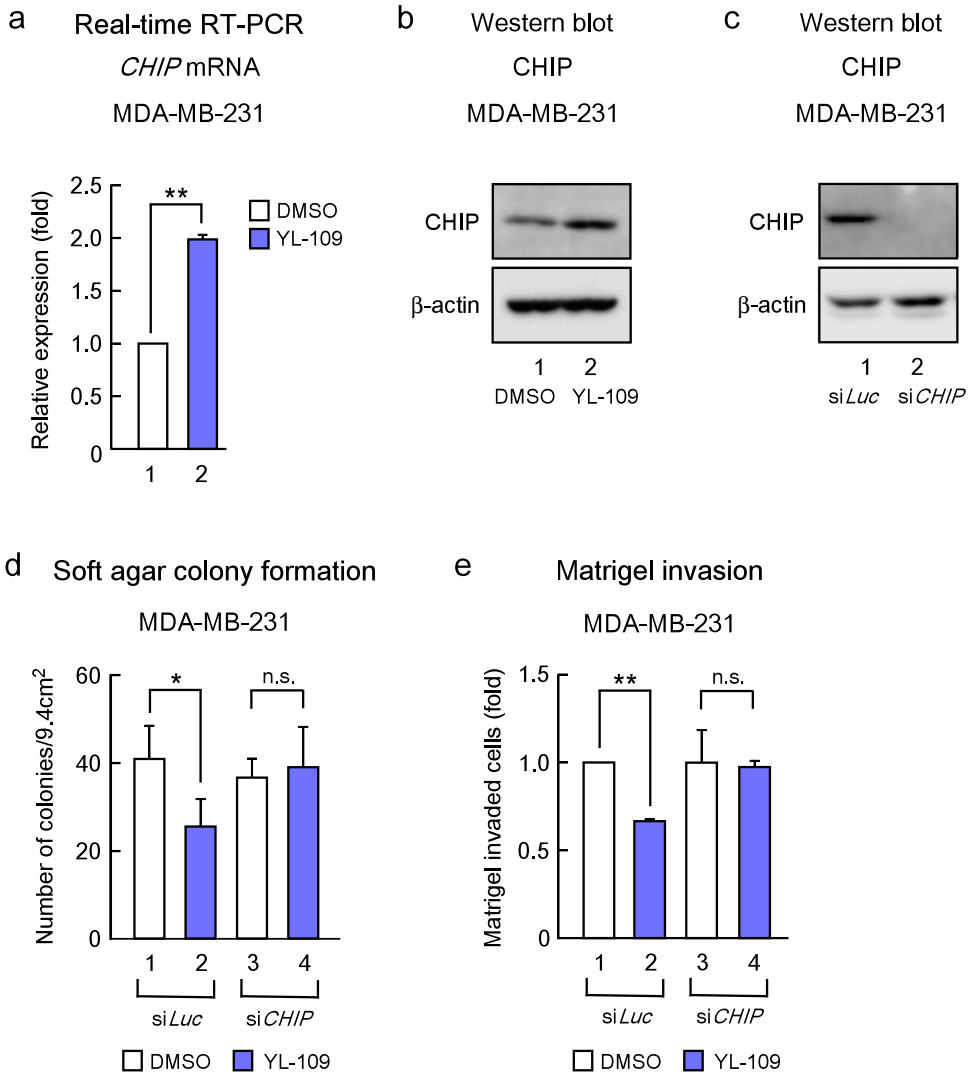

Figure 3 | YL-109 inhibits breast cancer progression by inducing CHIP expression. (a and b) Effect of YL-109 on CHIP levels in MDA-MB-231 cells. MDA-MB-231 cells were cultured in the absence or presence of YL-109 (1 μM). Total RNA was prepared from the indicated cells and the expression of *CHIP* was analyzed using real-time RT–PCR (a). Protein levels of CHIP were determined by Western blotting (b). Full length images of blots are represented in Supplementary Fig. S2. (c) Knock-down of CHIP by treatment with siRNA targeting CHIP. The levels of CHIP were examined by western blotting. Full length images of blots are represented in Supplementary Fig. S2. (d) Effects of CHIP knockdown on YL-109-induced reduction of anchorage-independent cell growth in MDA-MB-231 cells. CHIP expression was knocked down in MDA-MB-231 cells, and cells were plated in soft agar dishes in the absence or presence of YL-109 (1 μM). After incubation for 3 weeks, colonies were examined under a microscope and colonies with a diameter of more than 50 μm were counted. (e) Effects of CHIP knockdown on YL-109-reduced invasiveness in MDA-MB-231 cells. MDA-MB-231 cells were knocked down of CHIP and pre-cultured in the absence or presence of YL-109 (1 μM) for 48 h. The cells were seeded onto filters with Matrigel matrix-coated upper chambers in the absence or presence of YL-109 (1 μM). After 24 h incubation, invaded cells were stained using crystal violet. * indicates $p<0.05$, ** indicates $p<0.01$, and n.s. indicates $p>0.05$ by student's T test vs. DMSO-treated cells.

cells. These findings suggest that YL-109 may induce ERα degradation because of AhR activation in ER-positive breast cancer cells. Taken together, our results show that YL-109 suppresses cell growth through AhR signaling in both ER-positive and triple-negative breast cancer cells. In TNBC cells, YL-109 increases CHIP levels by AhR activation. In contrast, in ER-positive cells, YL-109 induces ERα degradation by AhR activation.

The treatment options for patients with TNBC, including those with ER-negative breast cancer, have not yet been established. In this study, we have demonstrated that YL-109 has antitumor activity in TNBC cells, and thus represents a potential TNBC therapy. In addition, resistance to anti-estrogens like tamoxifen is a major clinical problem in the treatment of hormone-dependent breast cancer including ER-positive breast cancer. Our results indicated that YL-109 inhibited tumor growth using a different mechanism from anti-estrogens in ER-positive breast cancer cells. Therefore, we predict that YL-109 will also exert an antitumor effect in tamoxifen-resistant breast cancer. Thus, YL-109 might have the ability to treat with several subtypes of breast cancer.

Drug resistance is a serious problem in breast cancer therapy, and cancer stem cells contributed to chemotherapeutic drug and radiation resistance[30]. Breast cancer stem cells form mammospheres and express stem cell markers. We observed that YL-109 markedly inhibited mammosphere formation and decreased the ALDH-positive cell population in MDA-MB-231 cells. Moreover, YL-109 significantly decreased *Klf-4* and *Hes1* expression in mammospheres derived from MDA-MB-231 cells. KLF-4 is essential for the maintenance of breast cancer stem cells and cell invasiveness[31], and Hes1 is a target of Notch signaling, which may be important for the self-renewal of breast cancer stem cells[32,33].

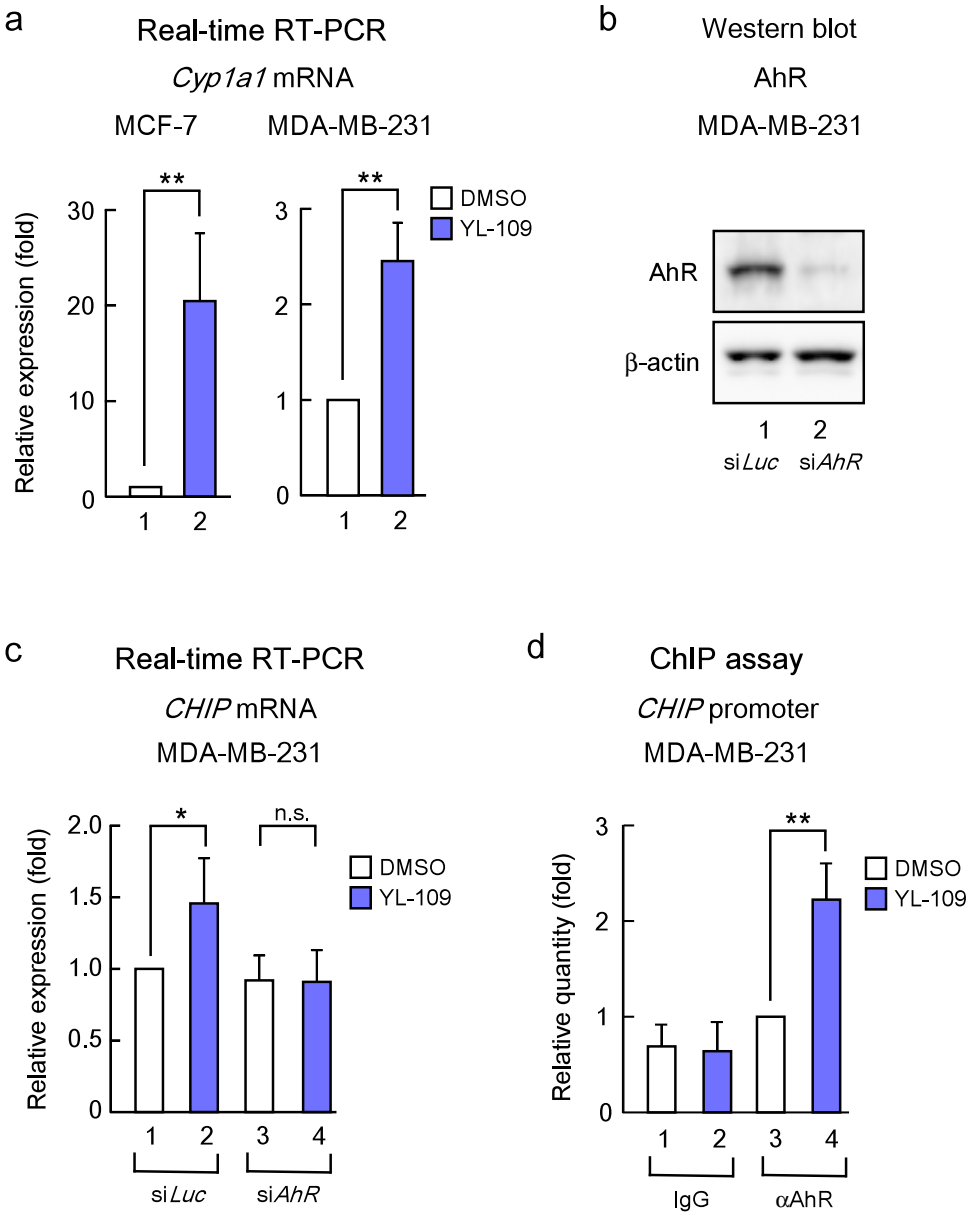

Figure 4 | YL-109 induces CHIP expression through AhR activation. (a) Effects of YL-109 on *Cyp1a1* mRNA expression in breast cancer cells. MCF-7 or MDA-MB-231 cells were cultured in the absence or presence of YL-109 (1 μM). *Cyp1a1* mRNA level was quantified using real-time RT-PCRs. (b) Knockdown of AhR by treatment with siRNA targeting AhR. Western blotting was used to examine the levels of AhR. Full length images of blots are represented in Supplementary Fig. S2. The representative blots for AhR were cropped to clarify relevant bands. (c) Effects of AhR knockdown on YL-109-increased *CHIP* expression. AhR expression was knocked down in MDA-MB-231 cells, and cells were cultured in the absence or presence of YL-109 (1 μM). *CHIP* expression was analyzed using real-time RT-PCRs. (d) AhR recruitment to *CHIP* promoter by YL-109. MDA-MB-231 cells were cultured in the absence or presence of YL-109 (1 μM). ChIP assay was performed with control IgG or anti-AhR antibodies. Immunoprecipitated DNA was examined using real-time RT-PCR and primers specific for the *CHIP* promoter. Samples were normalized to the amount of input DNA. * indicates $p<0.05$, ** indicates $p<0.01$, and n.s. indicates $p>0.05$ by student's T test vs. DMSO-treated cells.

Therefore, our results suggest that YL-109 inhibits the properties of breast cancer stem cells and can be used for patients with drug-resistant cancer.

In summary, we demonstrated that YL-109 is a novel antitumor agent that suppresses tumor progression in TNBC cells and inhibits cancer stem cell properties, unlike other benzothiazoles. Furthermore, we show that YL-109 induces CHIP expression through AhR signaling. Taken together, we propose a new therapeutic strategy for breast cancer including TNBC, and prodrug of YL-109 improved water solubility and chemically stability may be helpful in development of new pharmacological treatments for TNBC.

Methods

Cell culture. MCF-7, MDA-MB-231 and BT-20 cells were maintained in Dulbecco's modified Eagle's medium (DMEM) or RPMI1640 supplemented with 10% fetal bovine serum (FBS). For the experiments, cells were seeded in phenol red-free DMEM containing 4% charcoal-stripped FBS. After 24 h, the medium was exchanged for phenol red-free DMEM containing 1% charcoal-stripped FBS with or without ligands.

RNA interference. For transfection of siRNAs, cells at 30–50% confluency were transfected with 20 nmol/L of siRNA using Lipofectamine RNAi max (Invitrogen) according to the manufacture's protocol. All siRNAs were purchased from Invitrogen. The siRNA duplexes

CHIP, 5′-CCAGCGCUCUUCGAAUCGCGAAGAA-3′;
AhR, 5′-GAGAAUUCUUAUUACAGGCUCUGAA-3′.

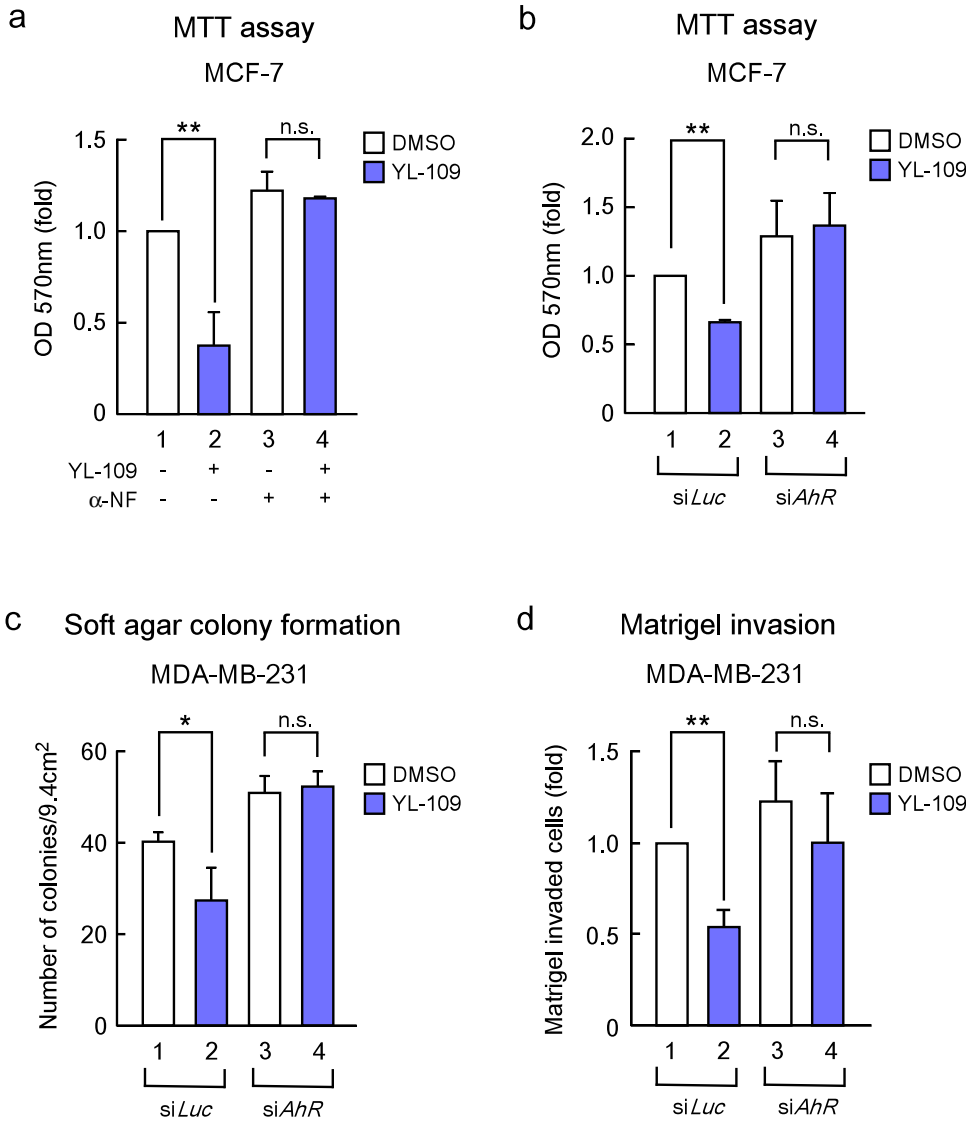

Figure 5 | YL-109 suppresses breast cancer progression through AhR signaling. (a and b) Effects of AhR on YL-109-inhibited cell proliferation in MCF-7 cells. MCF-7 cells were cultured in the absence or presence of YL-109 (1 μM), AhR antagonist α-NF (1 μM) (a). MCF-7 cells knocked down of AhR were cultured in the absence or presence of YL-109 (1 μM) (b). The cell viability was measured by MTT assays. (c) Effects of AhR knockdown on YL-109-inhibited anchorage-independent cell growth in MDA-MB-231 cells. AhR expression was knocked down in MDA-MB-231 cells, and cells were plated in soft agar dishes in the absence or presence of YL-109 (1 μM). After incubation for 3 weeks, colonies were examined under a microscope and colonies with a diameter of more than 50 μm were counted. (d) Effects of AhR knockdown on YL-109-reduced invasiveness in MDA-MB-231 cells. MDA-MB-231 cells were seeded onto filters with Matrigel matrix-coated upper chambers in the absence or presence of YL-109 (1 μM). * indicates $p<0.05$, ** indicates $p<0.01$, and n.s. indicates $p>0.05$ by student's T test vs. DMSO-treated cells.

Stealth™ RNAi reporter control was used as a negative control.

MTT assay. Cells were incubated in DMEM containing 4% charcoal-stripped FBS with DMSO or YL-109 (1 μM) for 96 h. The proliferation of cultured cells was measured by MTT assay using the MTT Cell Count Kit (Nakarai tesque).

Poly-HEMA. One gram of poly-(2-hydroxyethyl methacrylate) (poly-HEMA) (Sigma-Aldrich) was dissolved in 25 mL 99.5% ethanol and mixed overnight at 37°C. The poly-HEMA stock solution were added to 12-well plates and plates were left to dry for a few hours. After drying, the plates were washed with PBS. Cells were plated in the poly-HEMA-coated 12-well plates at a density of 1×10^5 cells (MCF-7) or 1.5×10^5 cells (MDA-MB-231) per well and incubated for 24 h. Cells were treated with 0.2% trypan blue. Viable cells were counted using Countess Automated Cell Counter (Invitrogen).

Soft agar colony-formation assay. For soft agar assays, 2×10^5 cells were suspended in DMEM containing 0.35% agar and layered on top of 1 mL of DMEM solidified with 0.6% agar in each well of a 6-well plate. After growing at 37°C for 3 weeks, colonies were counted under the microscope. The reported results represent the averages of three independent experiments.

Invasion and migration assay. The invasive potentials of MDA-MB-231 and BT-20 cells were tested with Matrigel invasion chambers (24-well format, 8 μm pore size; BD Biosciences). After incubation in DMEM containing 1% charcoal-stripped FBS with DMSO or YL-109 (1 μM) for 48 h, suspensions (0.5 mL) containing 1×10^5 cells (MDA-MB-231) or 0.5×10^5 cells (BT-20) were added with vehicle alone (DMSO) or YL-109 (1 μM), and transferred into insert chambers. These cells were then incubated for 24 h at 37°C with 0.75 mL of DMEM containing 4% charcoal-stripped FBS and each ligand in the bottom chambers. After incubation, the cells on the upper surface of the filter were removed, and invading cells were fixed in methanol. Fixed cells were stained with crystal violet and counted under a microscope. Migration assays were performed using the same procedure, except that the insert chambers were not coated with Matrigel and cells in chamber were incubated for 12 h.

Tumor xenograft models. BALB/cAjcl-nu/nu female mice at 4-5 weeks of age were purchased from CLEA Japan. The mice were kept in a pathogen-free environment under controlled conditions of light and humidity. MCF-7 or MDA-MB-231 cells were cultured as monolayers, trypsinized and resuspend in Matrigel (BD Biosciences) at each 1×10^8 or 1×10^7 cells/ml. Each mouse was injected subcutaneously with 100 μL of cell suspension (1×10^7 or 1×10^6 cells) in both flanks. YL-109 was subcutaneously injected in the scruff of the neck (15 mg/kg) for every 2 days. Tumor growth was

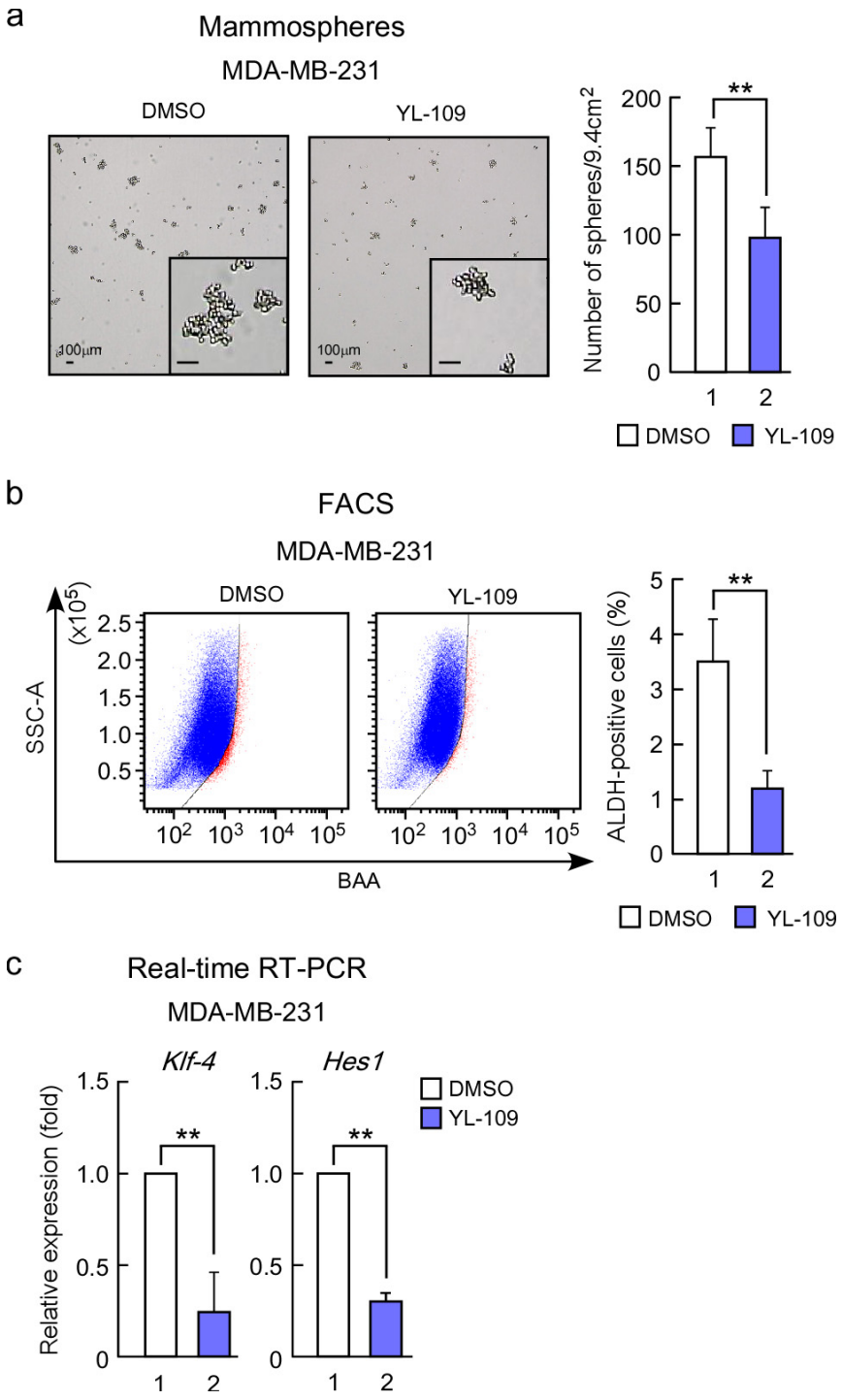

Figure 6 | YL-109 reduces cancer stem cell properties in MDA-MB-231 cells. (a) Effects of YL-109 on Mammosphere formation. MDA-MB-231 cells were inoculated onto ultra-low-attachment plates in the absence or presence of YL-109 (1 μM. After 7 days, mammospheres with a diameter of more than 100 μm were counted. The photographs in the left panel show representative mammospheres. The insets in panels show magnified images. The scale bars represent 100 μm. The graph in right panel shows the number of mammospheres. (b) Effects of YL-109 on ALDH-positive cell population. MDA-MB-231 cells were incubated with YL-109 (1 μM) for 96 h and ALDH-positive cell population was measured by the Aldefluor assay kit and flow cytometry. (c) Effects of YL-109 on the expression of cancer stem cell markers in mammospheres. The mammospheres were collected after 7 days culture on ultra-low-attachment plates in the absence or presence of YL-109 (1 μM). The gene expressions of *Klf-4* and *Hes1* were analyzed using real-time RT-PCR. ** indicates $p<0.01$ by student's T test vs. DMSO-treated cells.

monitored twice each week by measuring the tumor size using calipers; tumor volume was determined using the formula $V=1/2 \times$ larger diameter $\times$ (smaller diameter)^2. All animal experiments were performed in accordance with institutional guidelines.

In vivo lung metastasis analysis. BALB/cAjcl-nu/nu female mice at 4-5 weeks of age were purchased from CLEA Japan. The tail vein of each mouse was injected with MDA-MB-231 cells (5×10^5 cells). Forty-two days after injection, the mice were sacrificed and lung metastases were examined by hematoxylin-eosin (H&E) staining and immunohistochemistry for human cytokeratin and quantified by real-time RT-PCRs using primers specific for human *HPRT* that did not cross-react with the mouse homologue. Mouse β-actin was used for normalization.

Immunohistochemistry. Immunohistochemistry was performed under contract with Genostaff Co., Ltd. Tissues were fixed, dehydrated and embedded in paraffin

were cut at 5 μm thickness. For antigen retrieval, the sections were incubated with EDTA buffer [10 mM Tris-HCl and 1 mM ethylenediaminetetraacetic acid (EDTA)] (pH 9.0) at 95°C for 20 min, and then treated with 0.3% hydrogen peroxide. After blocking, the sections were incubated with anti-human-cytokeratin clone MNF-116 (Abcam) (10 μg/ml, overnight at 4°C). Immunostaining was performed with EnVision™ system (Dako). Staining of H&E was performed by standard protocol.

Real-time RT-PCR. Tissues and cells were homogenized in 1 mL of Sepazol and total RNA was extracted according to the manufacturer's instructions (Nacalai tesque). cDNA was synthesized from total RNA using RevaTraAce reverse transcriptase (Toyobo) and oligo dT primer. Real-time PCRs were performed to amplify fragments representing for the indicated mRNA expression using the Thermal Cycle DiceTM TP800 (Takara) and SYBR Premix Ex Taq (Takara). The primer sequences can be found in Supplementary Table S1.

Western blotting. Cells were lysed in TNE buffer [10 mM Tris-HCl (pH 7.8), 1% Nonidet P-40 (NP-40), 0.15 M NaCl, and 1 mM EDTA], and then immunoblotted with the appopriate antibodies. A murine hybridoma monoclonal antibody against human CHIP was generated in our laboratory. The antibodies used in this study were: anti- human CHIP (1 : 500; Green Space Biomed, Japan), AhR (1 : 500; Santa Cruz), and β-actin (1 : 5000; Sigma) antibodies. Specific proteins were visualized using an enhanced chemiluminescence (ECL) Western blot detection system (Millipore).

Chromatin immunoprecipitation (ChIP) assay. This was done essentially as described previously[34]. The DNA was amplified by real-time PCR as described above. The primers for real-time PCR are as follows: forward primer: 5′-TCACATGCTTCTCTGCTCTG-3′; reverse primer: 5′-GACTGTTGGTAGAGTGGAAG-3′ for *CHIP* gene upstream region. Samples were normalized based on the amount of input DNA.

Mammosphere formation assay. MDA-MB-231 cells were plated onto 6-well ultra-low-attachment plates (Corning Costar) at 5×10^3 cells per well. Cells were maintained in serum-free with a CnT-27 medium and growth additives (CellnTEC Advanced cell systems)[27]. After 7 days, over 100 μm spheres were counted.

ALDH assays. The ALDEFLUOR kit (Stem Cell Technologies, Durham, NC, USA) was used to detect cancer stem cell population with high aldehyde dehydrogenase (ALDH) enzyme activity, as previously reported[35]. Briefly, MDA-MB-231 cells were treated with YL-109 (1 μM) for 4 days. The cells were then incubated in ALDH assay buffer containing the ALDH substrate (BAAA, 1 μM) for 30 min at 37°C. As a negative control, cells were stained under identical conditions in the presence of diethylaminobenzaldehyde (DEAB, 15 μM), a specific ALDH inhibitor. FACS Aria II cell sorter (BD Biosciences) was used to measure the ALDH-positive cell population.

Statistical analysis. Data are representative of at least three different experiments. Significance of differences was determined by Student t-test analyses or by two-way ANOVA with Bonferroni's post hoc test (tumor xenograft experiments).

1. Foulkes, W. D., Smith, I. E. & Reis-Filho, J. S. Triple-negative breast cancer. *N. Engl. J. Med.* **363**, 1938–1948 (2010).
2. Perou, C. M. *et al.* Molecular portraits of human breast tumours. *Nature* **406**, 747–752 (2000).
3. Dent, R. *et al.* Triple-negative breast cancer: clinical features and patterns of recurrence. *Clin. Cancer Res.* **13**, 4429–4434 (2007).
4. Wicha, M. S., Liu, S. & Dontu, G. Cancer stem cells: an old idea--a paradigm shift. *Cancer Res.* **66**, 1883–1890; discussion 1895–1886 (2006).
5. Morrison, B. J., Schmidt, C. W., Lakhani, S. R., Reynolds, B. A. & Lopez, J. A. Breast cancer stem cells: implications for therapy of breast cancer. *Breast Cancer Res.* **10**, 210 (2008).
6. Xin, H. *et al.* CHIP controls the sensitivity of transforming growth factor-beta signaling by modulating the basal level of Smad3 through ubiquitin-mediated degradation. *J. Biol. Chem.* **280**, 20842–20850 (2005).
7. Kamynina, E., Kauppinen, K., Duan, F., Muakkassa, N. & Manor, D. Regulation of proto-oncogenic dbl by chaperone-controlled, ubiquitin-mediated degradation. *Mol. Cell Biol.* **27**, 1809–1822 (2007).
8. Fan, M., Park, A. & Nephew, K. P. CHIP (carboxyl terminus of Hsc70-interacting protein) promotes basal and geldanamycin-induced degradation of estrogen receptor-alpha. *Mol. Endocrinol.* **19**, 2901–2914 (2005).
9. Kajiro, M. *et al.* The ubiquitin ligase CHIP acts as an upstream regulator of oncogenic pathways. *Nat. Cell Biol.* **11**, 312–319 (2009).
10. Poland, A., Glover, E. & Kende, A. S. Stereospecific, high affinity binding of 2,3,7,8-tetrachlorodibenzo-p-dioxin by hepatic cytosol. Evidence that the binding species is receptor for induction of aryl hydrocarbon hydroxylase. *J. Biol. Chem.* **251**, 4936–4946 (1976).
11. Rowlands, J. C. & Gustafsson, J. A. Aryl hydrocarbon receptor-mediated signal transduction. *Crit. Rev. Toxicol.* **27**, 109–134 (1997).
12. Castro-Rivera, E., Wormke, M. & Safe, S. Estrogen and aryl hydrocarbon responsiveness of ECC-1 endometrial cancer cells. *Mol. Cell Endocrinol.* **150**, 11–21 (1999).
13. Wormke, M., Castro-Rivera, E., Chen, I. & Safe, S. Estrogen and aryl hydrocarbon receptor expression and crosstalk in human Ishikawa endometrial cancer cells. *J. Steroid Biochem. Mol. Biol.* **72**, 197–207 (2000).
14. Morrow, D., Qin, C., Smith, R., 3rd & Safe, S. Aryl hydrocarbon receptor-mediated inhibition of LNCaP prostate cancer cell growth and hormone-induced transactivation. *J. Steroid Biochem. Mol. Biol.* **88**, 27–36 (2004).
15. Koliopanos, A. *et al.* Increased arylhydrocarbon receptor expression offers a potential therapeutic target for pancreatic cancer. *Oncogene* **21**, 6059–6070 (2002).
16. Jana, N. R. *et al.* Comparative effects of 2,3,7,8-tetrachlorodibenzo-p-dioxin on MCF-7, RL95-2, and LNCaP cells: role of target steroid hormones in cellular responsiveness to CYP1A1 induction. *Mol. Cell. Biol. Res. Commun.* **4**, 174–180 (2000).
17. McDougal, A., Wormke, M., Calvin, J. & Safe, S. Tamoxifen-induced antitumorigenic/antiestrogenic action synergized by a selective aryl hydrocarbon receptor modulator. *Cancer Res.* **61**, 3902–3907 (2001).
18. Callero, M. A. & Loaiza-Perez, A. I. The role of aryl hydrocarbon receptor and crosstalk with estrogen receptor in response of breast cancer cells to the novel antitumor agents benzothiazoles and aminoflavone. *Int. J. Breast cancer* **2011**, 923250 (2011).
19. Trapani, V. *et al.* DNA damage and cell cycle arrest induced by 2-(4-amino-3-methylphenyl)-5-fluorobenzothiazole (5F 203, NSC 703786) is attenuated in aryl hydrocarbon receptor deficient MCF-7 cells. *Br. J. Cancer* **88**, 599–605 (2003).
20. Loaiza-Perez, A. I. *et al.* Aryl hydrocarbon receptor mediates sensitivity of MCF-7 breast cancer cells to antitumor agent 2-(4-amino-3-methylphenyl) benzothiazole. *Mol. Pharmacol.* **61**, 13–19 (2002).
21. Bradshaw, T. D. *et al.* Preclinical evaluation of amino acid prodrugs of novel antitumor 2-(4-amino-3-methylphenyl)benzothiazoles. *Mol. Cancer Ther.* **1**, 239–246 (2002).
22. Safe, S., Qin, C. & McDougal, A. Development of selective aryl hydrocarbon receptor modulators for treatment of breast cancer. *Expert Opin. Investig. Drugs* **8**, 1385–1396 (1999).
23. Wang, X. *et al.* Comparative properties of the nuclear aryl hydrocarbon (Ah) receptor complex from several human cell lines. *Eur. J. Pharmacol.* **293**, 191–205 (1995).
24. Wang, W. L., Porter, W., Burghardt, R. & Safe, S. H. Mechanism of inhibition of MDA-MB-468 breast cancer cell growth by 2,3,7,8-tetrachlorodibenzo-p-dioxin. *Carcinogenesis* **18**, 925–933 (1997).
25. Patani, N., Jiang, W., Newbold, R. & Mokbel, K. Prognostic implications of carboxyl-terminus of Hsc70 interacting protein and lysyl-oxidase expression in human breast cancer. *J. Carcinog.* **9**, 9 (2010).
26. Tsuchiya, M. *et al.* Ubiquitin ligase CHIP suppresses cancer stem cell properties in a population of breast cancer cells. *Biochem. Biophys. Res. Commun.* **452**, 928–932 (2014).
27. Prud'homme, G. J. *et al.* Breast cancer stem-like cells are inhibited by a non-toxic aryl hydrocarbon receptor agonist. *PLoS One* **5**, e13831 (2010).
28. Wormke, M., Stoner, M., Saville, B. & Safe, S. Crosstalk between estrogen receptor alpha and the aryl hydrocarbon receptor in breast cancer cells involves unidirectional activation of proteasomes. *FEBS Lett.* **478**, 109–112 (2000).
29. Wormke, M. *et al.* The aryl hydrocarbon receptor mediates degradation of estrogen receptor alpha through activation of proteasomes. *Mol. Cell Biol.* **23**, 1843–1855 (2003).
30. Wang, J., Guo, L. P., Chen, L. Z., Zeng, Y. X. & Lu, S. H. Identification of cancer stem cell-like side population cells in human nasopharyngeal carcinoma cell line. *Cancer Res.* **67**, 3716–3724 (2007).
31. Yu, F. *et al.* Kruppel-like factor 4 (KLF4) is required for maintenance of breast cancer stem cells and for cell migration and invasion. *Oncogene* **30**, 2161–2172 (2011).
32. Dontu, G. *et al.* Role of Notch signaling in cell-fate determination of human mammary stem/progenitor cells. *Breast Cancer Res.* **6**, R605–615 (2004).
33. Harrison, H. *et al.* Regulation of breast cancer stem cell activity by signaling through the Notch4 receptor. *Cancer Res.* **70**, 709–718 (2010).
34. Ito, I. *et al.* A nonclassical vitamin D receptor pathway suppresses renal fibrosis. *J. Clin. Invest.* **123**, 4579–4594 (2013).
35. Hirata, N., Sekino, Y. & Kanda, Y. Nicotine increases cancer stem cell population in MCF-7 cells. *Biochem. Biophys. Res. Commun.* **403**, 138–143 (2010).

Acknowledgments

The authors are grateful to Professor Shin-ichi Hayashi (Tohoku University), Professor Masafumi Kurosumi, Dr. Yuri Yamaguchi (Saitama Cancer Center) and Professor Akiyoshi Fukamizu (University of Tsukuba) for their technical support and helpful suggestions. This work was supported by a Grant-in-Aid from the Ministry of Education, Culture Sports, Science and Technology of Japan (MEXT; KAKENHI Grant number 25893022 to HH, and KAKENHI Grant number 26670041 to YK), a Program for Promotion of Fundamental Studies in Health Sciences of the National Institute of Biomedical Innovation (NIBIO), Japan to YK, KN, and JY, and Takeda Science Foundation to JY.

Author contributions

H.H. and J.Y. supervised the project and designed the study. H.H. and N.G. performed a most of the experimental work. M.T., N.H. and Y.K. performed some of the experiments.

K.I. and K.N. synthesized the compound. H.H., N.G., Y.N. and J.Y. wrote the manuscript. All authors reviewed the manuscript.

Additional information

Supplementary information accompanies this paper at http://www.nature.com/scientificreports

Competing financial interests: The authors declare no competing financial interests.

How to cite this article: Hiyoshi, H. *et al.* 2-(4-Hydroxy-3-methoxyphenyl)-benzothiazole suppresses tumor progression and metastatic potential of breast cancer cells by inducing ubiquitin ligase CHIP. *Sci. Rep.* **4**, 7095; DOI:10.1038/srep07095 (2014).

Biochemical and Biophysical Research Communications 452 (2014) 928–932

Contents lists available at ScienceDirect

Biochemical and Biophysical Research Communications

journal homepage: www.elsevier.com/locate/ybbrc

Ubiquitin ligase CHIP suppresses cancer stem cell properties in a population of breast cancer cells

Mai Tsuchiya [a], Yuka Nakajima [a,b], Naoya Hirata [c], Tamaki Morishita [a], Hiroyuki Kishimoto [a,b], Yasunari Kanda [c], Keiji Kimura [a,*]

[a] Graduate School of Life and Environmental Sciences, University of Tsukuba, Tsukuba Science City, Ibaraki 305-8572, Japan
[b] Life Science Center of Tsukuba Advanced Research Alliance, University of Tsukuba, Tsukuba Science City, Ibaraki 305-8572, Japan
[c] Division of Pharmacology, National Institute of Health Sciences, 1-18-1 Kamiyoga, Setagya-ku, Tokyo 158-8501, Japan

ARTICLE INFO

Article history:
Received 29 August 2014
Available online 16 September 2014

Keywords:
CHIP
Cancer stem cell
Breast cancer

ABSTRACT

Cancer stem cells (CSCs) have several distinctive characteristics, including high metastatic potential, tumor-initiating potential, and properties that resemble normal stem cells such as self-renewal, differentiation, and drug efflux. Because of these characteristics, CSC is regarded to be responsible for cancer progression and patient prognosis. In our previous study, we showed that a ubiquitin E3 ligase carboxyl terminus of Hsc70-interacting protein (CHIP) suppressed breast cancer malignancy. Moreover, a recent clinical study reported that CHIP expression levels were associated with favorable prognostic parameters of patients with breast cancer. Here we show that CHIP suppresses CSC properties in a population of breast cancer cells. CHIP depletion resulted in an increased proportion of CSCs among breast cancers when using several assays to assess CSC properties. From our results, we propose that inhibition of CSC properties may be one of the functions of CHIP as a suppressor of cancer progression.

1. Introduction

Breast cancer is the most frequent cause of cancer death among women [1]. Although numerous therapeutic strategies have been developed for breast cancer, many problems with achieving complete remission remain to be resolved.

In a previous study we showed that a ubiquitin E3 ligase carboxyl terminus of Hsc70-interacting protein (CHIP) suppressed breast cancer malignancy [2]. CHIP is a tetratricopeptide repeat (TPR) containing protein that is expressed in a number of organs [3,4]. CHIP ubiquitinates misfolded proteins along with heat shock proteins and induces their degradation through the proteasome pathway, which is involved in protein quality control [5–7]. Moreover, CHIP participates in several biological processes through ubiquitination of specific target proteins [8–10]. In our previous study, we found that CHIP expression levels were negatively correlated with tumor malignancy in human breast tissues and suppressed tumor growth and metastasis of breast cancer cells [2]. In addition, a recent clinical study reported that CHIP expression levels were associated with favorable prognostic parameters of patients with breast cancer [11]. Thus, CHIP may be a novel target for breast cancer therapy. However, many issues remain to be addressed regarding the mechanism(s) of how CHIP is involved in breast cancer progression.

Recent studies suggested the importance of eliminating cancer stem cells (CSCs) to achieve complete remission [12,13]. CSCs have tumor-initiating potential [14] and high metastatic potential [15]. They also have properties that resemble those of normal stem cells, such as self-renewal, differentiation [16], and drug efflux [17]. Because of their self-renewal and differentiation properties, CSCs organize into a hierarchical structure and give rise to cancer heterogeneity [16], which hampers prediction of tumor behavior and clinical outcome [18]. Moreover, these cells' drug efflux capability results in resistance to conventional chemotherapies, which allows CSCs to survive even under anticancer drug treatment conditions [17]. Thus, understanding the biology of CSCs would contribute to the development of novel cancer therapies by overcoming problems encountered clinically, such as therapeutic resistance and relapse.

CSC properties can be assessed using different specific experimental systems; such as a sphere formation assay, a side

Abbreviations: CHIP, carboxyl terminus of Hsc70-interacting protein; CSC, cancer stem cell; SP, side population.

* Corresponding author at: University of Tsukuba, 1-1-1 Tenno-dai, Tsukuba Science City, Ibaraki 305-8577, Japan. Fax: +81 29 853 6439.
E-mail address: kekimura@tara.tsukuba.ac.jp (K. Kimura).

http://dx.doi.org/10.1016/j.bbrc.2014.09.011
0006-291X/

population (SP) assay, and a limiting dilution xenograft assay. These assays are based on stem cell-like characteristics; including non-adherent growth capability [19] and drug efflux capacity [20], and on tumor-initiating potential [14]. To assess the non-adherent growth capability, the sphere formation assay is conducted [19]. In this assay, cancer cells are cultured under non-adherent conditions and form some spheres [21], after which the numbers of spheres are counted. To examine the drug efflux capacity mediated by transporters, the SP assay has been used [20]. In this assay, the proportions of SP cells are determined by evaluating the efflux capacity for the DNA-binding dye Hoechst 33342 using a fluorescence-activated cell sorter (FACS) [20]. To test the tumor-initiating potential, the limiting dilution xenograft assay is conducted [14,22]. While non-CSCs cannot form tumors by themselves, CSCs can initiate tumors *in vivo* [22]. This tumor-initiating potential is assessed by transplantation of serial diluted cancer cells into immunodeficient mice.

Numerous studies analyzed the CSC properties using breast cancer cell lines [21,23]. Clinically, breast cancer cells with stem cell phenotypes were also detected in bone marrow of breast cancer patients [24]. Thus, the presence of CSCs among breast cancer cells is becoming clear, but the precise regulation and characteristics of CSCs remains to be determined.

Here we show that depleting CHIP increases the proportions of CSCs among breast cancer cells by examining CSC properties using these assays. Thus, CHIP may contribute to a favorable prognosis for patients with breast cancer through its inhibition of CSC properties.

2. Materials and methods

2.1. Cell culture and treatment

MCF-7, MDA-MB-231 and T47D cells were maintained in Dulbecco's modified Eagle's medium (DMEM) supplemented with 10% fetal bovine serum (FBS) and Penicillin-Streptomycin Mixed Solution (Nacalai Tesque).

2.2. RNA interference

RNA interference experiment was performed as described in Kajiro et al. [2], with minor modification. We used a retroviral expression system. The pVSV-G vector and pSINsi-hU6 (Takara) vector containing either the *CHIP* or *LacZ* (control) target sequence were co-transfected into GP2-293 cells (Clontech). MCF-7 and T47D cells were incubated with the retroviral supernatant in the presence of 8 μg/ml polybrene. Twenty-four hours after infection, the viral supernatant was replaced with fresh DMEM containing 10% FBS. The infected cells were selected with 1 mg/ml G418. The target sequences were 5′-gcacgacaagtacatggcgga-3′ for *CHIP*, and 5′-gctacacaaatcagcgatt-3′ for *LacZ*.

2.3. Immunoblotting

Immunoblotting experiment was performed as described in Kajiro et al. [2]. Cells were lysed in 0.5% Triton buffer [50 mM Tris-HCl (pH 7.5), 150 mM NaCl, 0.5 mM EDTA, and 0.5% TritonX-100]. Extracted proteins were separated by SDS–PAGE, transferred onto PVDF membranes (Millipore), immunoblotted with the indicated antibodies. The antibodies employed in this study included mouse monoclonal antibodies specific for β-Actin (1:1000; Santa Cruz, clone C4), and rat monoclonal antibodies against human CHIP (1:250; Green Space Biomed, Japan).

2.4. Sphere forming assay

MCF-7 cells were plated onto 6-well ultra-low-attachment plates (Corning Costar) at 1000 cells per well. MCF-7 cells were maintained in DMEM/Ham's F-12 (Nacalai Tesque) supplemented with 0.4% bovine serum albumin, 4 μg/ml bovine insulin (Sigma-Aldrich), 20 ng/ml EGF (Peprotech), and 1 × B27 supplement (Gibco). After 7 days, over 100 μm spheres were counted using BioZero BZ8000 microscope (Keyence). T47D cells were plated onto 6-well ultra-low-attachment plates at 5000 cells per well. T47D cells were maintained in CnT-27 medium (Cellntec). After 10 days culture, over 100 μm spheres were counted. MDA-MB-231 cells were plated onto 6-well ultra-low-attachment plates at 5000 cells per well. MDA-MB-231 cells were maintained in CnT-Prime medium (Cellntec). After 7 days culture, over 100 μm spheres were counted.

2.5. Side population (SP) analysis

Cells were removed from culture dish by Tripsin-EDTA solution. 1×10^6 cells were suspended in 970 μl Hanks' balanced salt solution (HBSS) with 2% fetal bovine serum (FBS) and 10 mM HEPES (pH 7.4). The cells were incubated at 37°C for 90 minutes with 17.5 μg/ml Hoechst 33342 (Sigma-Aldrich). Then, the cells were washed with 2% FBS in PBS, and resuspended in ice-cold HBSS with 2% FBS, 10 mM HEPES (pH 7.4), and 2 μg/ml propidium iodide (Sigma-Aldrich). Fumitremorgin C (FTC, 1 μM) was used to confirm the SP fraction. SP cells were analyzed with FACSAria (BD Biosciences). Collected events were analyzed using FlowJo (Tree Star).

2.6. Real-time RT-PCR

Real-time RT-PCR was performed as described in Kajiro et al. [2], with minor modification. Cells were homogenized in 1 ml of Sepasol-RNA I Super G (Nacalai Tesque) and total RNA was extracted according to the instruction manual and treated with DNase (Promega) for 30 min at 37°C. cDNA was synthesized from total RNA using RevatraAce reverse transcriptase (Toyobo) and random primers. The cDNA was amplified by rea-ltime PCR using Thermal Cycler Dice™ TP800 (Takara) and SYBR® Premix Ex Taq™ (Takara). Samples were normalized by *PPIA* mRNA levels. The primers for real-time PCR are as follows: 5′-acgtggtataaaaggggcgg-gag-3′ and 5′-tcaccaccctgacacataaaccctg-3′ for *PPIA*, 5′-atgcctgt-gatttgtgggcc-3′ and 5′-gccagttgtttttctgccac-3′ for *NANOG*, and 5′-ggacccattggcattctc-3′ and 5′-caggacacagcatagaataatc-3′ for *CD133*.

2.7. Limiting dilution transplantation assay

NOD.CB17-*Prkdc*^{scid}/J (NOD/SCID) female mice at 5 weeks of age were purchased from Charles River Laboratories US. MCF-7 cells were cultured as monolayers, trypsinized, and resuspended in Matrigel (BD Biosciences) at dose ranging from 1.0×10^6 to 5.0×10^2 cells/ml. Female NOD/SCID mice were given bilateral subcutaneous injections of 0.1 ml MCF-7 cells. The mice were kept in a pathogen-free environment. After 6 weeks all of the mice were sacrificed, and the tumor tissues were collected. All animal experiments were in accordance with institutional guidelines.

2.8. Statistical analysis

Student's *t*-test was used to compare number of sphere (Fig. 1C and E) and mRNA levels (Fig. 3). Standard deviation and sample number were abbreviated as "S.D." and "*n*", respectively.

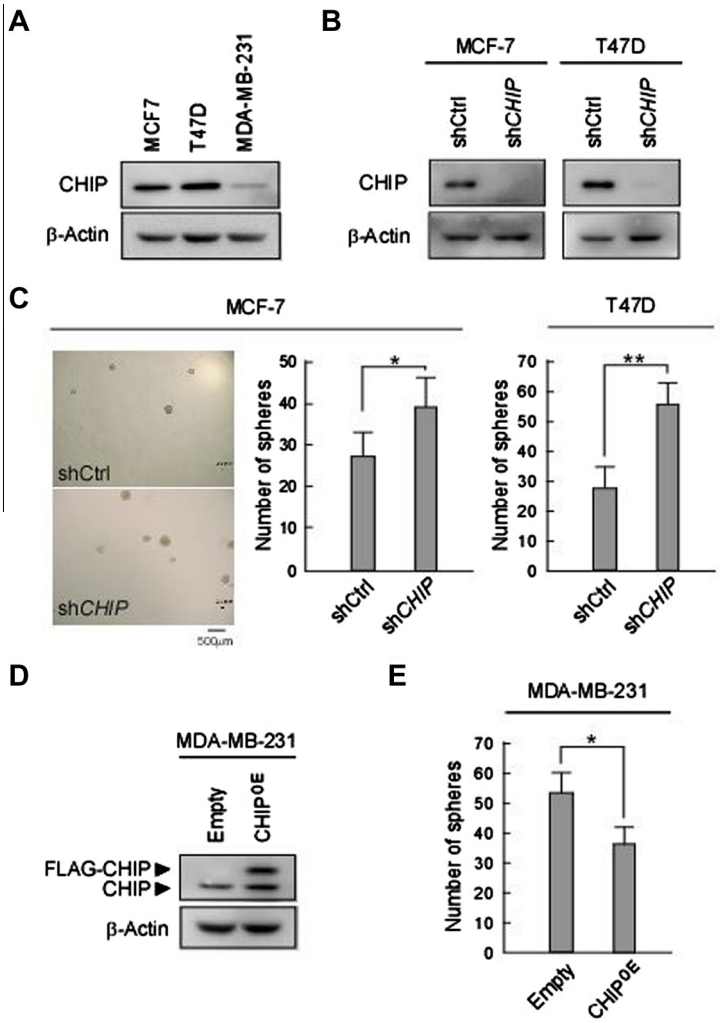

Fig. 1. CHIP inhibits sphere-forming capability. (A) Endogenous CHIP expression levels in MCF-7, T47D, and MDA-MB-231 cells. Total cell lysates of these cells were analyzed using the indicated antibodies. (B) CHIP depletion efficiency by shRNA. CHIP protein levels in MCF-7 and T47D cells infected with a retro virus containing shRNA against *LacZ* (shCtrl) and *CHIP* (sh*CHIP*) were analyzed by immunoblotting using the indicated antibodies. (C) Sphere-forming capabilities of MCF-7 and T47D shCtrl and sh*CHIP* cells. Representative photomicrographs (left panels) and numbers of spheres (right graphs) are shown. (D) CHIP protein levels in MDA-MB-231 cells introduced FLAG-CHIP ($CHIP^{OE}$) or empty vector (empty). Cells were generated as described by Kajiro et al [2]. CHIP expression levels were assessed using the indicated antibodies. (E) Sphere-forming capabilities of MDA-MB-231 empty and $CHIP^{OE}$ cells. Numbers of spheres (right graphs) are shown. Error bars are + S.D.; $n = 3$ for C and E. $^{*}p < 0.05$; $^{**}p < 0.01$.

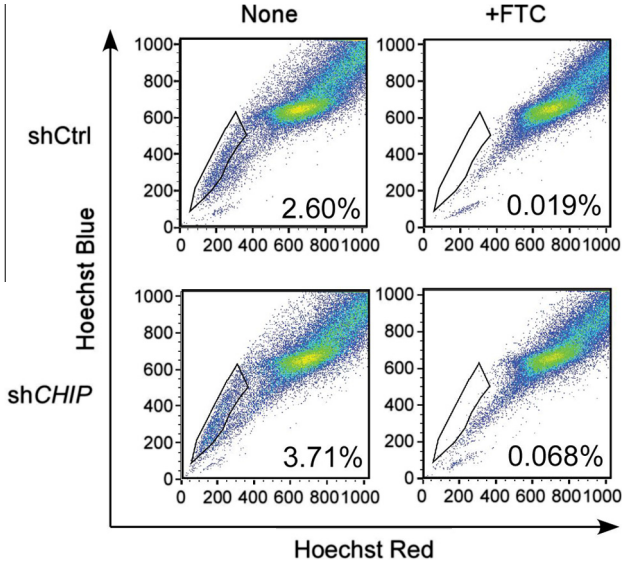

Fig. 2. CHIP depletion increases the proportion of SP cells. Fumitremorgin C (FTC) was used to confirm the SP fraction. SP cells were detected using FACS analysis.

3. Results

CHIP expression levels were previously found to be significantly associated with the prognosis of patients with breast cancer [11]. Consistent with this clinical observation, CHIP expression levels in MCF-7 and T47D cell lines, both non-aggressive human breast cancer cell lines, were much higher than in the MDA-MB-231 cell line, an aggressive triple-negative human breast cancer cell line (Fig. 1A). However, little is known regarding the mechanism(s) of how CHIP is involved in breast cancer progression. Therefore, we investigated the relationship between CHIP expression levels and CSC properties, as recent evidence suggests that CSCs are responsible for cancer progression and recurrence [12,13].

We first analyzed sphere-forming capability, which is one of the major indices used to define CSCs [19], to test the effects of CHIP depletion on CSC properties. When CHIP expression levels were reduced using shRNA for *CHIP* (sh*CHIP*) in MCF-7 and T47D cells (Fig. 1B), sphere formation assay results showed that sh*CHIP* cells more frequently formed spheres than did shCtrl cells both for MCF-7 and T47D cells (Fig. 1C). Alternatively, we used FLAG-tagged CHIP over-expressed MDA-MB-231 cells ($CHIP^{OE}$; Fig. 1D), as

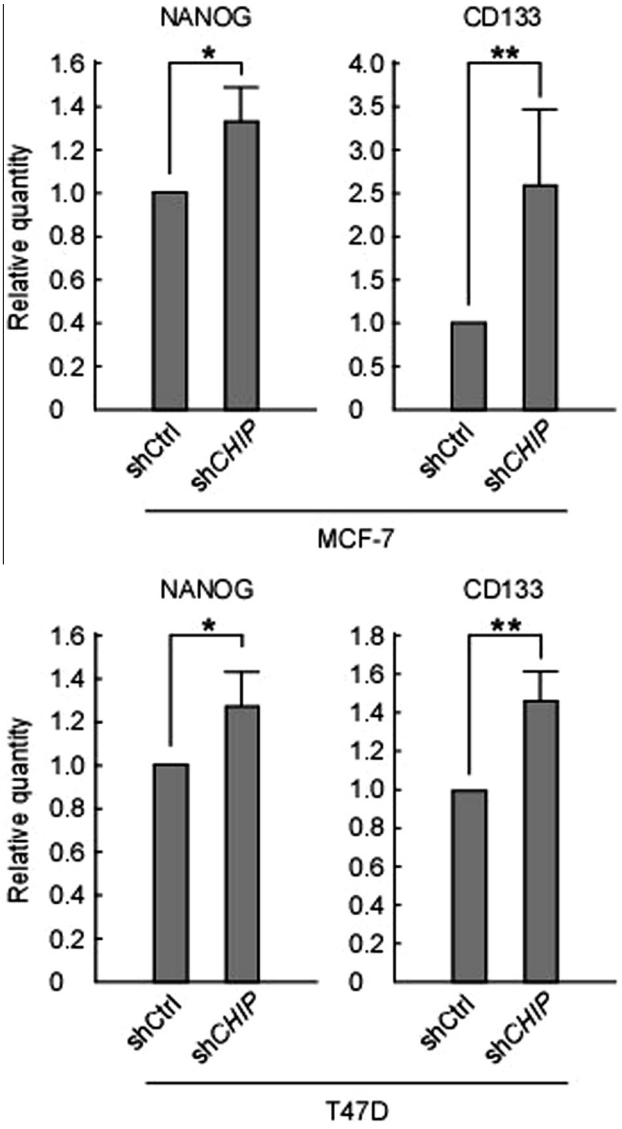

Fig. 3. mRNA levels of CSC related genes are enhanced in spheres after CHIP depletion. Error bars are +S.D.; $n \geqslant 3$. $^{*}p < 0.05$; $^{**}p < 0.01$.

described by Kajiro et al. [2], to further test the effect of CHIP expression on sphere-forming capability. Consistent with the CHIP depletion results, sphere-forming capability was reduced for CHIP^{OE} MDA-MB-231 cells (Fig. 1E). Taken together, these results (Fig. 1) indicated that CHIP expression levels were negatively correlated with sphere-forming capability, which suggested that CHIP suppressed CSC phenotypes.

We next analyzed the proportion of the SP fraction in sh*CHIP* cells to further assess whether CHIP suppressed CSC phenotypes. SP assay is one method used to assess CSC enrichment in several cancers, including breast cancer [25], hepatocellular carcinoma [26], ovarian cancer [27], and lung cancer [28]. SP cells, which have the ability to efflux the DNA-binding dye Hoechst 33342 out of the cell membranes, were detected using FACS analysis [20]. This showed that the proportion of the SP fraction in sh*CHIP* cells was markedly higher than that of shCtrl cells (Fig. 2); thus, CHIP depletion had increased the SP fraction in breast cancer cells.

We then tested whether CHIP depletion affected the expression levels of CSC-related genes. We isolated total RNAs from spheres derived from MCF-7 or T47D shCtrl and sh*CHIP* cells and analyzed the expression levels of some CSC-related genes. As a result, CHIP depletion increased the expression levels of self-renewal gene NANOG [29] and cell surface marker gene CD133 [23,29,30] in spheres (Fig. 3), suggesting that CSC-related genes such as NANOG and CD133 were involved in enhanced CSC properties by CHIP depletion.

Table 1
Tumor initiation capability of MCF-7 cells is enhanced by CHIP depletion.

Number of cell line	Number of cells injected				
	10^5	10^4	10^3	10^2	50
shCtrl	4/4	4/4	3/4	1/4	0/4
sh*CHIP*	4/4	4/4	4/4	4/4	1/4

Finally, we examined whether tumor-initiating potential was affected by CHIP expression levels, as numerous studies have indicated that CSCs have tumor-initiating potential [14]. To examine this, we conducted a limiting dilution xenograft assay using NOD/SCID mice. This showed that tumors were more effectively initiated in MCF-7 sh*CHIP* cells than in shCtrl cells (Table 1), which demonstrated that the tumor-initiating capability was increased in CHIP-depleted cells.

All of these results showed that CHIP depletion increased the CSC population among breast cancer cells (Figs. 1–3 and Table 1). Thus, CHIP may reduce breast cancer malignancy by suppressing CSC properties.

4. Discussion

In our previous study, we found that CHIP suppressed breast cancer metastasis and tumor growth. Moreover, a clinical study reported that CHIP expression levels were associated with a favorable prognosis for patients with breast cancer [11]. All of these findings suggest that CHIP suppresses breast cancer malignancy.

In this study, using several different assays, we found that CHIP depletion increased the CSC population among non-aggressive breast cancer cell lines that had higher CHIP protein levels, whereas CHIP over-expression reduced the CSC population in an aggressive breast cancer cell line that had lower CHIP protein expression. Thus, inhibition of CSC properties by CHIP may account for one aspect of CHIP as a suppressor of cancer progression, because CSCs have high metastatic [15] and tumor-initiating potentials [14]. Thus, it is possible that inhibition of CSC properties by CHIP could result in a favorable prognosis for patients with breast cancer with higher CHIP expression. However, we have not yet determined the molecular mechanism(s) of how CHIP suppresses CSC properties.

We consider that there are two possibilities for inhibition of CSC properties by CHIP, one is by quantity control and the other is quality control of proteins due to its ubiquitinating potential. Numerous studies have identified CSC-related genes, including transcription factors [31,32], receptors [33,34], and signaling factors [35,36]. Thus, the abundance of one or some of these CSC-related factors may be regulated by CHIP (quantity control), as CHIP regulates the quantity of its specific substrates by inducing protein degradation [2,9,10]. Alternatively, the accumulation of misfolded proteins due to CHIP depletion may cause for the changes in the expression of genes that function to maintain CSC properties, as CHIP regulates protein quality by inducing the degradation of misfolded proteins [5–7]. Our next goals will be to identify the target proteins of CHIP and elucidate the molecular mechanisms of how CHIP suppresses CSC properties.

In this study, we showed that CHIP suppressed not only breast cancer metastasis and tumor growth [2], but also CSC properties. Thus, developing methods to enhance CHIP expression levels may provide an efficient therapy for patients with breast cancer.

Therefore, understanding the relationship between CHIP expression and CSC properties and regulating its expression may provide important clues for developing a novel breast cancer therapy.

Acknowledgment

The authors would like to thank Enago (www.enago.jp) for the English language review.

This work was supported by grants from the Ministry of Education, Culture, Sports, Science and Technology of Japan.

References

[1] J. Ferlay, H.R. Shin, F. Bray, D. Forman, C. Mathers, D.M. Parkin, Estimates of worldwide burden of cancer in: GLOBOCAN 2008, Int. J. Cancer 127 (2010) (2008) 2893–2917.
[2] M. Kajiro, R. Hirota, Y. Nakajima, K. Kawanowa, K. So-ma, I. Ito, Y. Yamaguchi, S.H. Ohie, Y. Kobayashi, Y. Seino, M. Kawano, Y. Kawabe, H. Takei, S. Hayashi, M. Kurosumi, A. Murayama, K. Kimura, J. Yanagisawa, The ubiquitin ligase CHIP acts as an upstream regulator of oncogenic pathways, Nat. Cell Biol. 11 (2009) 312–319.
[3] C.A. Ballinger, P. Connell, Y. Wu, Z. Hu, L.J. Thompson, L.Y. Yin, C. Patterson, Identification of CHIP, a novel tetratricopeptide repeat-containing protein that interacts with heat shock proteins and negatively regulates chaperone functions, Mol. Cell. Biol. 19 (1999) 4535–4545.
[4] H. McDonough, C. Patterson, CHIP: a link between the chaperone and proteasome systems, Cell Stress Chaperones 8 (2003) 303–308.
[5] J. Jiang, C.A. Ballinger, Y. Wu, Q. Dai, D.M. Cyr, J. Hohfeld, C. Patterson, CHIP is a U-box-dependent E3 ubiquitin ligase: identification of Hsc70 as a target for ubiquitylation, J. Biol. Chem. 276 (2001) 42938–42944.
[6] S. Murata, Y. Minami, M. Minami, T. Chiba, K. Tanaka, CHIP is a chaperone-dependent E3 ligase that ubiquitylates unfolded protein, EMBO Rep. 2 (2001) 1133–1138.
[7] A.L. Goldberg, Protein degradation and protection against misfolded or damaged proteins, Nature 426 (2003) 895–899.
[8] L. Li, H. Xin, X. Xu, M. Huang, X. Zhang, Y. Chen, S. Zhang, X.Y. Fu, Z. Chang, CHIP mediates degradation of Smad proteins and potentially regulates Smad-induced transcription, Mol. Cell. Biol. 24 (2004) 856–864.
[9] A. Lazorchak, M.E. Jones, Y. Zhuang, New insights into E-protein function in lymphocyte development, Trends Immunol. 26 (2005) 334–338.
[10] C.H. Woo, N.T. Le, T. Shishido, E. Chang, H. Lee, K.S. Heo, D.M. Mickelsen, Y. Lu, C. McClain, T. Spangenberg, C. Yan, C.A. Molina, J. Yang, C. Patterson, J. Abe, Novel role of C terminus of Hsc70-interacting protein (CHIP) ubiquitin ligase on inhibiting cardiac apoptosis and dysfunction via regulating ERK5-mediated degradation of inducible cAMP early repressor, FASEB J. 24 (2010) 4917–4928.
[11] N. Patani, W. Jiang, R. Newbold, K. Mokbel, Prognostic implications of carboxyl-terminus of Hsc70 interacting protein and lysyl-oxidase expression in human breast cancer, J. Carcinog. 9 (2010) 9.
[12] R.J. Jones, Cancer stem cells-clinical relevance, J. Mol. Med. (Berlin) 87 (2009) 1105–1110.
[13] K. Eppert, K. Takenaka, E.R. Lechman, L. Waldron, B. Nilsson, P. van Galen, K.H. Metzeler, A. Poeppl, V. Ling, J. Beyene, A.J. Canty, J.S. Danska, S.K. Bohlander, C. Buske, M.D. Minden, T.R. Golub, I. Jurisica, B.L. Ebert, J.E. Dick, Stem cell gene expression programs influence clinical outcome in human leukemia, Nat. Med. 17 (2011) 1086–1093.
[14] M. Al-Hajj, M.F. Clarke, Self-renewal and solid tumor stem cells, Oncogene 23 (2004) 7274–7282.
[15] F. Li, B. Tiede, J. Massague, Y. Kang, Beyond tumorigenesis: cancer stem cells in metastasis, Cell Res. 17 (2007) 3–14.
[16] J.E. Visvader, G.J. Lindeman, Cancer stem cells: current status and evolving complexities, Cell Stem Cell 10 (2012) 717–728.
[17] M. Dean, ABC transporters, drug resistance, and cancer stem cells, J. Mammary Gland Biol. Neoplasia 14 (2009) 3–9.
[18] E.M.F. De Sousa, L. Vermeulen, E. Fessler, J.P. Medema, Cancer heterogeneity – a multifaceted view, EMBO Rep. 14 (2013) 686–695.
[19] M. Cariati, A. Naderi, J.P. Brown, M.J. Smalley, S.E. Pinder, C. Caldas, A.D. Purushotham, Alpha-6 integrin is necessary for the tumourigenicity of a stem cell-like subpopulation within the MCF7 breast cancer cell line, Int. J. Cancer 122 (2008) 298–304.
[20] C. Wu, B.A. Alman, Side population cells in human cancers, Cancer Lett. 268 (2008) 1–9.
[21] Y. Glinka, N. Mohammed, V. Subramaniam, S. Jothy, G.J. Prud'homme, Neuropilin-1 is expressed by breast cancer stem-like cells and is linked to NF-kappaB activation and tumor sphere formation, Biochem. Biophys. Res. Commun. 425 (2012) 775–780.
[22] M. Al-Hajj, M.S. Wicha, A. Benito-Hernandez, S.J. Morrison, M.F. Clarke, Prospective identification of tumorigenic breast cancer cells, Proc. Natl. Acad. Sci. U.S.A. 100 (2003) 3983–3988.
[23] M.H. Wright, A.M. Calcagno, C.D. Salcido, M.D. Carlson, S.V. Ambudkar, L. Varticovski, Brca1 breast tumors contain distinct CD44+/CD24- and CD133+ cells with cancer stem cell characteristics, Breast Cancer Res. 10 (2008) R10.
[24] M. Balic, H. Lin, L. Young, D. Hawes, A. Giuliano, G. McNamara, R.H. Datar, R.J. Cote, Most early disseminated cancer cells detected in bone marrow of breast cancer patients have a putative breast cancer stem cell phenotype, Clin. Cancer Res. 12 (2006) 5615–5621.
[25] L. Patrawala, T. Calhoun, R. Schneider-Broussard, J. Zhou, K. Claypool, D.G. Tang, Side population is enriched in tumorigenic, stem-like cancer cells, whereas ABCG2+ and ABCG2− cancer cells are similarly tumorigenic, Cancer Res. 65 (2005) 6207–6219.
[26] T. Chiba, K. Kita, Y.W. Zheng, O. Yokosuka, H. Saisho, A. Iwama, H. Nakauchi, H. Taniguchi, Side population purified from hepatocellular carcinoma cells harbors cancer stem cell-like properties, Hepatology 44 (2006) 240–251.
[27] P.P. Szotek, R. Pieretti-Vanmarcke, P.T. Masiakos, D.M. Dinulescu, D. Connolly, R. Foster, D. Dombkowski, F. Preffer, D.T. Maclaughlin, P.K. Donahoe, Ovarian cancer side population defines cells with stem cell-like characteristics and mullerian inhibiting substance responsiveness, Proc. Natl. Acad. Sci. U.S.A. 103 (2006) 11154–11159.
[28] M.M. Ho, A.V. Ng, S. Lam, J.Y. Hung, Side population in human lung cancer cell lines and tumors is enriched with stem-like cancer cells, Cancer Res. 67 (2007) 4827–4833.
[29] C.R. Jeter, B. Liu, X. Liu, X. Chen, C. Liu, T. Calhoun-Davis, J. Repass, H. Zaehres, J.J. Shen, D.G. Tang, NANOG promotes cancer stem cell characteristics and prostate cancer resistance to androgen deprivation, Oncogene 30 (2011) 3833–3845.
[30] J.X. Cheng, B.L. Liu, X. Zhang, How powerful is CD133 as a cancer stem cell marker in brain tumors?, Cancer Treat Rev. 35 (2009) 403–408.
[31] F. Yu, J. Li, H. Chen, J. Fu, S. Ray, S. Huang, H. Zheng, W. Ai, Kruppel-like factor 4 (KLF4) is required for maintenance of breast cancer stem cells and for cell migration and invasion, Oncogene 30 (2011) 2161–2172.
[32] J. Yang, D. Liao, C. Chen, Y. Liu, T.H. Chuang, R. Xiang, D. Markowitz, R.A. Reisfeld, Y. Luo, Tumor-associated macrophages regulate murine breast cancer stem cells through a novel paracrine EGFR/Stat3/Sox-2 signaling pathway, Stem Cells 31 (2013) 248–258.
[33] C. Ginestier, S. Liu, M.E. Diebel, H. Korkaya, M. Luo, M. Brown, J. Wicinski, O. Cabaud, E. Charafe-Jauffret, D. Birnbaum, J.L. Guan, G. Dontu, M.S. Wicha, CXCR1 blockade selectively targets human breast cancer stem cells in vitro and in xenografts, J. Clin. Invest. 120 (2010) 485–497.
[34] M.P. Ablett, C.S. O'Brien, A.H. Sims, G. Farnie, R.B. Clarke, A differential role for CXCR4 in the regulation of normal versus malignant breast stem cell activity, Oncotarget 5 (2014) 599–612.
[35] J.E. Visvader, G.J. Lindeman, Cancer stem cells in solid tumours: accumulating evidence and unresolved questions, Nat. Rev. Cancer 8 (2008) 755–768.
[36] G.K. Malhotra, X. Zhao, H. Band, V. Band, Shared signaling pathways in normal and breast cancer stem cells, J. Carcinog. 10 (2011) 38.

J Pharmacol Sci 124, 000 – 000 (2014)

Journal of Pharmacological Sciences

Full Paper

Assessment of Testing Methods for Drug-Induced Repolarization Delay and Arrhythmias in an iPS-Derived Cardiomyocyte Sheet: Multi-site Validation Study

Yuji Nakamura[1], Junko Matsuo[1,2,3], Norimasa Miyamoto[4], Atsuko Ojima[4], Kentaro Ando[1], Yasunari Kanda[2], Kohei Sawada[4], Atsushi Sugiyama[1,*a], and Yuko Sekino[2,5,*b]

[1]*Department of Pharmacology, Faculty of Medicine, Toho University, Tokyo 143-8540, Japan*
[2]*Division of Pharmacology, National Institute of Health Sciences, Tokyo 158-8501, Japan*
[3]*Drug Safety Research Laboratories, Shin Nippon Biomedical Laboratories, Ltd., Japan*
[4]*Biopharmaceutical Assessments Core Function Unit, Eisai Product Creation Systems, Eisai Co., Ltd., Japan*
[5]*Department of Neurobiology and Behavior, Gunma University Graduate School of Medicine, Gunma 371-8511, Japan*

Received November 26, 2013; Accepted February 11, 2014

Abstract. A prospective comparison study across 3 independent research laboratories of a pure I_{Kr} blocker E-4031 was conducted by using the same batch of human iPS cell–derived cardiomyocytes in order to verify the utility and reliability of our original standard protocol. Field potential waveforms were recorded with a multi-electrode array system to measure the inter-spike interval and field potential duration. The effects of E-4031 at concentrations of 1 to 100 nM were sequentially examined every 10 min. In each facility, E-4031 significantly prolonged the field potential duration corrected by Fridericia's formula and caused early after-depolarizations occasionally resulting in triggered activities, whereas it tended to decrease the rate of spontaneous contraction. These results were qualitatively and quantitatively consistent with previous non-clinical in vitro and in vivo studies as well as clinical reports. There were inter-facility differences in some absolute values of the results, which were not observed when the values were normalized as percentage change. Information described in this paper may serve as a guide when predicting the drug-induced repolarization delay and arrhythmias with this new technology of stem cells.

Keywords: E-4031, iPS cell–derived cardiomyocyte, multi-site validation, field potential, TdP

Introduction

Drug-induced proarrhythmia has been a major safety concern about the development of new drugs, leading to issuing of ICH E14 and S7B guidelines in May 2005 (1, 2). The guidelines have effectively reduced risks of a new compound causing torsades de pointes, whereas non-clinical and clinical studies in the current approach still remain imperfect because they identify many drugs as being "positive" despite a lack of demonstrable pro-arrhythmic risk (3 – 6). In a recent workshop held in July 2013 by the US Food and Drug Administration (FDA), the Cardiac Safety Research Consortium and the non-profit Health and Environmental Sciences Institute (HESI), a new paradigm was proposed and discussed, focusing on a comprehensive assessment of multi ion channel effects to determine actual proarrhythmic risk of drugs (7). This new approach will include a stem-cell technology that has the potential to improve the currently used assessment of cardiotoxicity; however, more work is required prior to the use of stem cell–derived cardiomyocyte models to accurately predict proarrhythmias in humans (7).

There have been a large number of various studies with stem cell–derived cardiomyocytes examining electrophysiological effects of drugs (8 – 13). In an effort to further improve upon the assay system, this report describes a more simple and reliable protocol of an induced pluripotent stem (iPS) cell–derived, cardio-

Corresponding authors.
*[a]atsushi.sugiyama@med.toho-u.ac.jp, *[b]yukos@nihs.go.jp
Published online in J-STAGE
doi: 10.1254/jphs.13248FP

myocyte-sheet model. Extensive preliminary studies have confirmed that the protocol proposed in this paper could be optimal for assessing E-4031-induced repolarization delay and arrhythmias and would qualitatively and quantitatively reflects its electropharmacological profile in humans. This is a critically new finding and a significant improvement over the previous in vitro I_{Kr} assay systems including the hERG potassium channels and the papillary muscle of guinea pigs. In this study, in order to start verifying the reproducibility of our protocol, a prospective comparison study of E-4031 was conducted across 3 independent research laboratories with the same batch of iPS cell–derived cardiomyocytes.

Materials and Methods

Cell culture and plating

Each facility (E, N, T) obtained the same batch (#1089404) of cryopreserved human iPS cell–derived cardiomyocytes [iCells; Cellular Dynamics International (CDI), Madison, WI, USA]. The cells were thawed in specially prepared medium (Plating Media, CDI), which were plated onto 0.1% gelatin-coated, 6-well tissue-culture plates (Becton Dickinson, Franklin Lakes, NJ, USA) at a density of $1.3 - 2.6 \times 10^6$ (E: 1.3×10^6, N: 2.0×10^6, T: $2.4 - 2.6 \times 10^6$) of cells per well. Two days after plating, Plating Media was replaced to specially prepared culture medium (Maintenance Media, CDI). Then, the culture medium was changed with fresh one every 2 days. The cells were cultured for 3.7 ± 1.4 days (2 – 7 days) after thawing at 37°C with 5% CO_2 prior to re-plating.

The electrical activity of cardiomyocytes was measured by using our original protocol. Briefly, the recording area of probes with 64 of the recording electrodes (MED probe; MED-P515A, Alpha Med Scientific, Osaka) of the MED64 System (Alpha Med Scientific) was coated with 2 μL of fibronectin (50 μg in 1 mL of distilled water), which was incubated at 37°C for $\geq$ 1 h. The cells cultured in the 6-well tissue-culture plates were dispersed with 0.25% trypsin-EDTA or TrypLE Select, which were re-plated onto the MED probes at a density of 3×10^4 cells in a 2 μL of the culture medium. The cells were incubated at 37°C with 5% CO_2 for 2 – 18 h (E: 4 – 12 h, N: 2 – 18 h, T: 12 – 18 h) in moisture condition prior to filling each probe with 1 mL of the culture medium. The half volume or all of the culture medium of the probes was changed with the culture medium, which had been warmed to 37°C, every 2 days thereafter. The cells were cultured for 5.2 ± 1.6 days (3 – 7 days) to obtain a sheet of cardiomyocytes with spontaneous and synchronous electrical automaticity.

Field potentials (FPs) assay

Maintenance Media was used as a culture medium throughout the experiment. Prior to the measurement of FPs, cardiomyocyte sheets were equilibrated for $\geq$ 30 min in the CO_2 incubator in 1 or 2 mL of fresh culture media. After equilibration, the probes were kept at 36°C – 37°C with thermo-control systems and covered with a lid, through which aeration of 95% O_2 / 5% CO_2 gas was provided. FPs from spontaneously beating cardiomyocyte sheets were recorded and digitized at 20 kHz by using the MED64 System. The stability and constancy of the waveforms, inter-spike interval, and field potential duration (FPD) were confirmed for $\geq$ 20 min. FPD was defined as an interval from the initial sharp deflection to the peak of the dome (8). Using the information obtained in this observation period, we selected 3 – 6 electrodes, which would be suitable for continuous monitoring of the FP configuration consisting of spike and dome. After recording the basal control state, the effects of 1, 3, 10, 30, and 100 nM of E-4031 were assessed by adding stock solution cumulatively to the culture medium to obtain target concentrations. The final concentration of DMSO was limited to be < 0.6%, since DMSO at a concentration of < 0.6% has been reported to hardly affect any of the variables assessed in this study (8). At each concentration, the FP was recorded for $\geq$ 10 min and the last 30 beats were extracted as a dataset to analyze waveforms, inter-spike interval, and FPDs according to the previous report (8). The datasets of concentrations were excluded from the statistical analysis, when early after-depolarization and/or triggered activity were observed. Early after-depolarization was defined as deflection occurring at the plateau of the dome, and sharp deflection originating from early after-depolarization was judged as a triggered activity. FPD was corrected with Fridericia's formula, which was defined as the primary method of correction in this study [$FPDcF = FPD / (\text{inter-spike interval} / 1000)^{1/3}$] (14). The values of inter-spike interval and FPDcF from the last 30 waves at each concentration were averaged.

Drugs and chemicals

E-4031 was obtained from WAKO (Osaka) or synthetized at Eisai Co., Ltd. (Tsukuba). Gelatin was obtained from Sigma (St. Louis, MO, USA). Fibronectin was obtained from Becton Dickinson or Invitrogen (Carlsbad, CA, USA). Trypsin-EDTA and TrypLE Select were obtained from Invitrogen.

Data analyses and statistical assessment

In each experiment, one electrode that satisfied the following two conditions was chosen: 1) FP was recorded whole through the experiment, and 2) The amplitude of

the dome was the largest. The data were expressed as the mean ± S.E.M. The effects of the drug on inter-spike interval and FPDcF obtained in each facility were evaluated with the paired *t*-test or one-way repeated-measures analysis of variance (ANOVA) followed by Contrasts for mean values comparison between the baseline value (0 nM) and others. Meanwhile, inter-facility variability was assessed with one-way factorial ANOVA followed by Fisher's test or unpaired *t*-test. A P value < 0.05 was considered statistically significant.

Results

The effects of E-4031 in concentrations of 0, 1, 3, 10, 30, and 100 nM were examined in each facility, except that 1 nM was not performed in facility N. The number of preparations that can be used for the assessment of inter-spike interval, field-potential duration, and categorical analysis decreased due to the onset of early after-depolarization and/or triggered activity as the concentration of drug increased.

Inter-spike interval

The effects of the drug on the inter-spike interval (ms) are summarized in Fig. 1 (upper panel). The baseline values (0 nM) were 926 ± 44 ms in facility E, 1,216 ± 56 ms in facility N, and 956 ± 22 ms in facility T. Inter-facility difference was observed between N and E besides between N and T, which was not detected between E and T. No significant change from the respective baseline values was detected at 1, 3, or 10 nM in E and T and at 3 nM in N. Inter-facility difference was observed at 3 nM between N and E besides between N and T, which was not detected at any concentration between E and T. Meanwhile, the effects of the drug on the inter-spike interval (%) are summarized in Fig. 1 (lower panel). The significant increase was observed at 3 nM in N, which was not detected at 1, 3, or 10 nM in E or T, although the similar trend was observed. Inter-facility difference was not detected at any concentration.

Prolongation of field-potential duration

The effects of the drug on the FPDcF (ms) are summarized in Fig. 2 (upper panel) and typical tracings of field potential before and after the drug treatment are depicted in Fig. 3. The baseline values (0 nM) were 430 ± 12 ms in E, 443 ± 5 ms in N, and 320 ± 15 ms in T. Inter-facility difference was detected between T and E besides between T and N, which was not detected between E and N. FPDcF was prolonged at 3 and 10 nM in E and at 10 nM in T, which tended to be prolonged at 3 nM in N without statistical significance. Inter-facility difference was detected at 1, 3, and 10 nM between E and T and at 3 nM between N and T. Inter-facility difference was not detected at any concentration between E and N. Meanwhile, the effects of the drug on the FPDcF (%) are summarized in Fig. 2 (lower panel). FPDcF was prolonged at 3 and 10 nM in E and at 10 nM in T, whereas it tended to be prolonged at 3 nM in N without statistical significance. Inter-facility difference was not detected at any concentration.

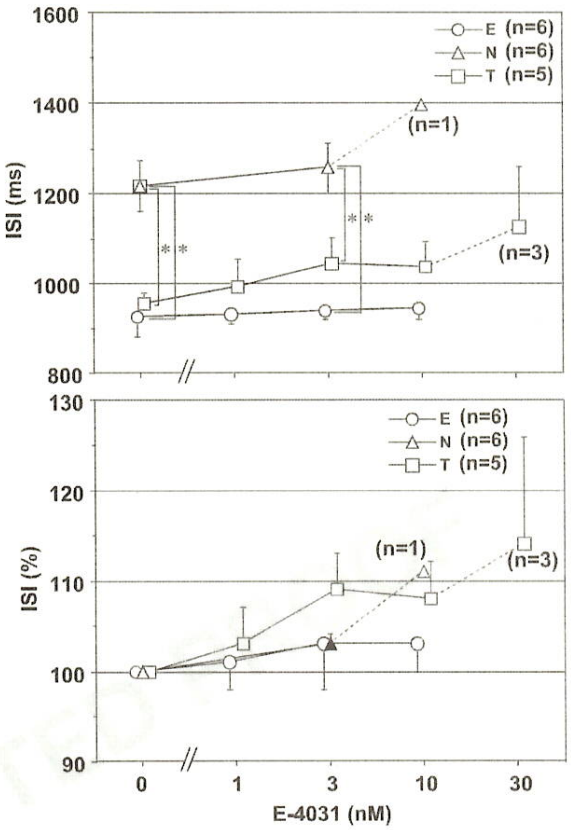

Fig. 1. Summary of the results showing the actual measurement values (upper) and their percentage changes (lower) in inter-spike interval (ISI) of E-4031 in human iPS cell–derived cardiomyocytes in each facility. Each value represents the mean ± S.E.M. of 6 preparations for facility E and facility N and 5 preparations for facility T. Values in parentheses represent the number of the preparations. An asterisk indicates significant difference between the facilities, whereas a closed symbol represents significant change from the respective baseline value.

Incidence of early after-depolarization or triggered activity

The incidence of early after-depolarization or triggered activity is summarized in Table 1 and typical tracing of field potential with triggered activity is depicted in

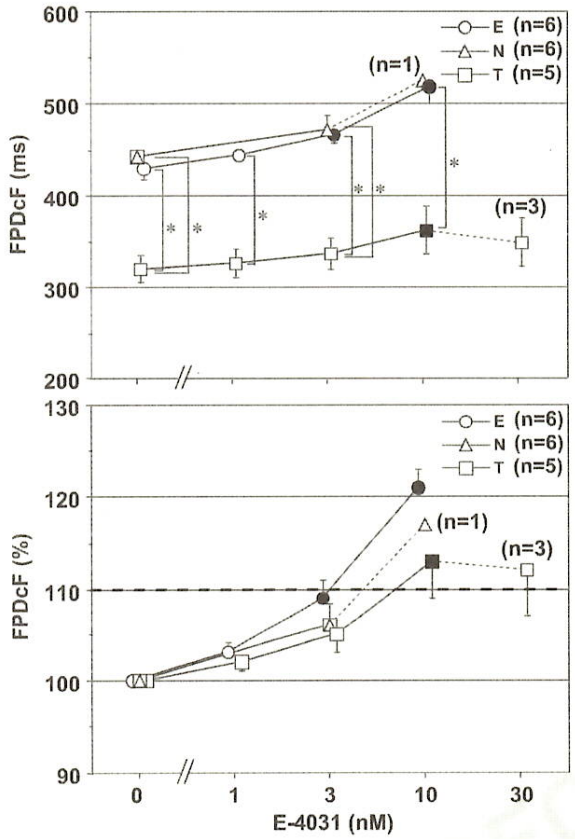

Fig. 2. Summary of the results showing the actual measurement values (upper) and their percentage changes (lower) in FPDcF of E-4031 in human iPS cell–derived cardiomyocytes in each facility. Each value represents the mean ± S.E.M. of 6 preparations for facility E and facility N and 5 preparations for facility T. Values in parentheses represent the number of the preparations. An asterisk indicates significant difference between facilities, whereas a closed symbol represents significant change from the respective baseline value.

Fig. 3. Early after-depolarization or triggered activity was induced at ≥ 10 nM in N and at ≥ 30 nM in E and T.

Categorical analysis of FPDcF

The results of categorical analysis of absolute FPDcF (ms) are summarized in Table 2. At the baseline and 1 nM, all FPDcF in each facility were categorized in ≤ 480 ms, whereas FPDcF of ≥ 500 ms was observed at ≥ 3 nM in N and at ≥ 10 nM in E, which was not observed in T.

The results of categorical analysis of ⊿FPDcF are summarized in Table 3. At 1 nM, all ⊿FPDcF in E and T were categorized in ≤ 60 ms. ⊿FPDcF of > 60 ms was observed at ≥ 3 nM in E and N and at ≥ 10 nM in T.

Discussion

In this study, a prospective comparison study of E-4031 was conducted with the same batch of human iPS cell–derived cardiomyocytes in order to start verifying the reproducibility of our original standard protocol across 3 independent research laboratories. We demonstrated that the protocol can be reliable in detecting the drug-induced repolarization delay and arrhythmias with high reproducibility.

E-4031 tended to show a negative chronotropic effect at concentrations of ≥ 3 nM; however, a significant change was detected only at 3 nM in facility N when assessed by percentage change (Fig. 1). A more potent negative chronotropic effect was observed by higher concentrations of E-4031 in each facility, although we did not perform the statistical analyses on inter-spike interval at concentrations of ≥ 10 nM in facility N and ≥ 30 nM in facilities E and T because of the limited number of experiments (n = 0 – 3). These results are in good accordance with a previous observation in patients with supraventricular tachyarrhythmias (15), in which E-4031 at a plasma concentration of 4.85 ± 1.35 ng/ml (11 nM) modestly prolonged RR interval, but it did not achieve statistical significance. Meanwhile in the single sinoatrial nodal cells of rabbits, E-4031 at a concentration of 100 nM suppressed or blocked the spontaneous activity (16), and moreover in the Langendorff-perfused whole hearts of guinea pig, E-4031 at concentrations of 30 – 300 nM or 5 μM significantly reduced the heart rate (17, 18). Thus, our testing method using the human iPS cell–derived cardiomyocytes can be considered to be more sensitive than currently available in vitro non-clinical models in detecting the E-4031-induced negative chronotropic effect.

E-4031 caused early after-depolarization and/or triggered activity in a concentration-related manner as shown in Fig. 3 and Table 1. In previous studies using the Langendorff-perfused rabbit heart, 0.5 μM of E-4031 induced early after-depolarization and triggered activity (19, 20). Also, in human embryonic stem cell–derived cardiomyocyte clusters, 1 μM of E-4031 induced early after-depolarization in half of the clusters (11). Meanwhile, in the human engineered heart tissue sheet made of the human embryonic stem cells, 10 nM of E-4031 was reported to induce arrhythmias (12). Thus, our testing method as well as the previous human engineered heart tissue sheet is considered to have higher sensitivities than the human cardiomyocyte clusters or the Langendorff-perfused rabbit heart in detecting E-4031-induced early after-depolarization and/or triggered activity.

E-4031 prolonged the FPDcF in a concentration-related manner as shown in Figs. 2 and 3. A wide variety

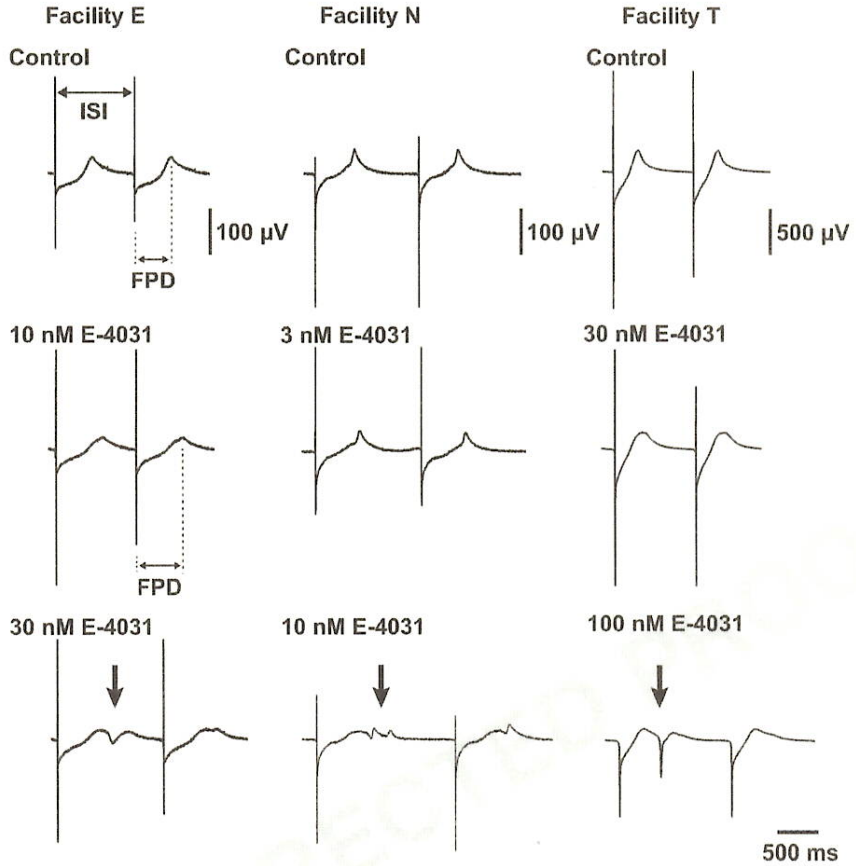

Fig. 3. Typical tracings of the field potential from each facility. Upper traces show the field potential at control (Control), middle traces indicate the prolongation of field potential duration (FPD) with 3 – 30 nM of E-4031, and lower traces represent the onset of early after-depolarization or triggered activity with 10 – 100 nM E-4031 (arrow). ISI: inter-spike interval.

Table 1. Incidence of E-4031-induced early afterdepolarization or triggered activity

Concentration (nM)	Facility			All
	E	N	T	
0	0% (0/6)	0% (0/6)	0% (0/5)	0% (0/17)
1	0% (0/6)	NT	0% (0/5)	0% (0/11)
3	0% (0/6)	0% (0/6)	0% (0/5)	0% (0/17)
10	0% (0/6)	83% (5/6)	0% (0/5)	29% (5/17)
30	100% (6/6)	100% (6/6)	40% (2/5)	82% (14/17)
100	100% (6/6)	100% (6/6)	100% (5/5)	100% (17/17)

Note: The numerator in parentheses shows the number of preparations exerting early after-depolarization or triggered activity, whereas the denominator indicates the total number of preparations assessed. NT: Not tested.

of analyses have been performed to clarify the effects of E-4031 on the repolarization process as summarized in Table 4 (12, 15, 17 – 26). The effects of E-4031 in these previous reports are directionally the same as the currently observed results, although their potency varied greatly. Thus, the present findings suggest that the sensitivity of current testing method to detect drug-induced repolarization delay can be considered to be comparable to hERG assay and human subjects, but it may be higher than those of in vivo and in vitro animal models.

Table 2. Summary of categorical analysis of absolute FPDcF values

Concentration of E-4031 (nM)	FPDcF (ms)	Facility			All
		E	N	T	
0	≤ 450	67% (4/6)	83% (5/6)	100% (5/5)	82% (14/17)
	> 450	33% (2/6)	17% (1/6)	0% (0/5)	18% (3/17)
	> 480	0% (0/6)	0% (0/6)	0% (0/5)	0% (0/17)
	> 500	0% (0/6)	0% (0/6)	0% (0/5)	0% (0/17)
1	≤ 450	50% (3/6)	NT	100% (5/5)	73% (8/11)
	> 450	50% (3/6)		0% (0/5)	27% (3/11)
	> 480	0% (0/6)		0% (0/5)	0% (0/11)
	> 500	0% (0/6)		0% (0/5)	0% (0/11)
3	≤ 450	17% (1/6)	17% (1/6)	100% (5/5)	41% (7/17)
	> 450	50% (3/6)	50% (3/6)	0% (0/5)	35% (6/17)
	> 480	33% (2/6)	17% (1/6)	0% (0/5)	18% (3/17)
	> 500	0% (0/6)	17% (1/6)	0% (0/5)	6% (1/17)
10	≤ 450	17% (1/6)	0% (0/1)	80% (4/5)	42% (5/12)
	> 450	0% (0/6)	0% (0/1)	20% (1/5)	8% (1/12)
	> 480	17% (1/6)	0% (0/1)	0% (0/5)	8% (1/12)
	> 500	67% (4/6)	100% (1/1)	0% (0/5)	42% (5/12)
30	≤ 450	— (0/0)	— (0/0)	100% (3/3)	100% (3/3)
	> 450	— (0/0)	— (0/0)	0% (0/3)	0% (0/3)
	> 480	— (0/0)	— (0/0)	0% (0/3)	0% (0/3)
	> 500	— (0/0)	— (0/0)	0% (0/3)	0% (0/3)

Note: The numerator in parentheses shows the number of preparations exerting respective FPDc values in each category, whereas the denominator indicates the total number of preparations assessed. FPDcF = FPD / (inter-spike interval / 1000)$^{1/3}$. NT: Not tested.

Table 3. Summary of categorical analysis of ΔFPDcF values

Concentration of E-4031 (nM)	ΔFPDcF (ms)	Facility			All
		E	N	T	
1	≤ 30	83% (5/6)	NT	100% (5/5)	91% (10/11)
	> 30	17% (1/6)		0% (0/5)	9% (1/11)
	> 60	0% (0/6)		0% (0/5)	0% (0/11)
3	≤ 30	67% (4/6)	67% (4/6)	100% (5/5)	76% (13/17)
	> 30	0% (0/6)	17% (1/6)	0% (0/5)	6% (1/17)
	> 60	33% (2/6)	17% (1/6)	0% (0/5)	18% (3/17)
10	≤ 30	0% (0/6)	0% (0/1)	60% (3/5)	25% (3/12)
	> 30	17% (1/6)	0% (0/1)	20% (1/5)	17% (2/12)
	> 60	83% (5/6)	100% (1/1)	20% (1/5)	58% (7/12)
30	≤ 30	— (0/0)	— (0/0)	33% (1/3)	33% (1/3)
	> 30	— (0/0)	— (0/0)	33% (1/3)	33% (1/3)
	> 60	— (0/0)	— (0/0)	33% (1/3)	33% (1/3)

Note: The numerator in parentheses shows the number of preparations exerting respective ΔFPDc values in each category, whereas the denominator indicates the total number of preparations assessed. ΔFPDcF: Increase from baseline in FPDcF. NT: Not tested.

Since 82% of the basal FPDcF was ≤ 450 ms, which is the upper limit of the normal range of QTc in human subjects, we examined the repolarization delays with the categorical analysis described in the ICH E14 guideline. FPDcF > 500 ms and/or ΔFPDcF > 60 ms were detected at concentrations of ≥ 3 nM in some preparations (Tables 2 and 3), indicating that 3 nM of E-4031 will be a critical concentration for inducing the excessive QT-interval prolongation by this testing method.

The major purpose of this study was to clarify the

Table 4. Summary of nonclinical and clinical reports regarding the effects of E-4031 on the repolarization markers

Model	Method	Marker	Change (%)	Concentration (nM)	References
hERG		IC_{50}		7.7	21
Guinea pig	Ventricular myocytes	APD_{90}	26	5,000	22
		APD_{90}	71	100	23
	Papillary muscles	APD_{70}	9 – 68	30 – 300	23
		APD_{90}	10	20	24
		APD_{30-90}	10	7	24
	Langendorff heart	QTc	5 – 27	3 – 300	18
		MAP_{90}	3 – 18	3 – 300	18
		QTc	26	5,000	17
Rabbit	Langendorff heart	QT	51	500	19
		MAP_{90}	50	500	19
Dog	In vivo (Anesthetized)	QT	57	6.2	25
		QTc	10	5.1	24
	In vivo (Conscious)	QTc	10	19.2	24
Monkey	In vivo (Conscious)	QTc	10	3.1	24
Human		QTc	14	12.1	15
		QTc	4.7 – 15	5.1 – 27	26
iPS cell	Single cell	APD_{90}	40 – 70	30 – 100	20
		APD_{90}	5 – 11	10 – 1,000	12
		APD_{30-90}	15 – 29	10 – 1,000	12

extent of the inter-facility difference in sensitivity and reliability of this new testing method. The concentrations of E-4031 that caused early after-depolarization and/or triggered activity were close to each other among the 3 facilities; however, there were some variations in the basal absolute values of inter-spike interval and FPDcF. Since we used the same batch of the cardiomyocytes, these differences might be induced by small inter-facility variability in the net culture period, the cell density on recording electrodes and/or experimental temperature. It should be noted that there was no difference in inter-spike interval or FPDcF among the 3 facilities when compared using percentage change.

In conclusion, we demonstrated that the use of the standardized protocol for the iPS cell–derived cardiomyocyte sheets can minimize inter-facility difference in detecting the drug-induced repolarization delay and arrhythmia. While further studies are needed to establish the currently proposed protocol including the assessment of variability across batches, more reference compounds and clinical predictability, information described in this paper may help predict the potential of the drug-induced repolarization delay and arrhythmias with this new technology. Also, methodological work for high-throughput evaluation is now ongoing.

Acknowledgments

This study was supported in part by the Research Promotion Grant from Toho University Graduate School of Medicine (No. 13-01) and a Regulatory Science Research Grant from the Ministry of Health Labour and Welfare. The authors thank Ms. Misako Nakatani, Ms. Tomoko Ohnishi, and Dr. Mitsuyoshi Luke Saito for their technical assistance and Alpha MED Scientific, Inc. and iPS Academia Japan, Inc. for their technical advice.

Conflicts of Interest

The authors declare no conflicts of interest.

References

1 ICH Harmonised Tripartite Guideline. The Non-clinical Evaluation of the Potential for Delayed Ventricular Repolarization (QT Interval Prolongation) by Human Pharmaceuticals S7B. Recommended for adoption at step 4 of the ICH process on 12 May 2005 by the ICH Steering Committee. ICH; (http://www.ich.org/fileadmin/Public_Web_Site/ICH_Products/Guidelines/Safety/S7B/Step4/S7B_Guideline.pdf)

2 ICH Harmonised Tripartite Guideline. The Clinical Evaluation of QT/QTc Interval Prolongation and Proarrhythmic Potential for Non-Antiarrhythmic Drugs E14. Recommended for adoption at step 4 of the ICH process on 12 May 2005 by the ICH Steering Committee. ICH; (http://www.ich.org/fileadmin/Public_Web_Site/

ICH_Products/Guidelines/Efficacy/E14/E14_Guideline.pdf)
3 Darpo B. The thorough QT study four years after the implementation of the ICH E14 guidance. Br J Pharmacol. 2010;159:49–57.
4 E14 Implementation Working Group ICH E14 Guideline: The Clinical Evaluation of QT/QTc Interval Prolongation and Proarrhythmic Potential for Non-Antiarrhythmic Drugs Questions & Answers (R1). 2012. (http://www.ich.org/fileadmin/Public_Web_Site/ICH_Products/Guidelines/Efficacy/E14/E14_Q_As_R1_step4.pdf)
5 Sugiyama A, Hashimoto H, Nakamura Y, Fujita T, Kumagai Y. QT/QTc study conducted in Japanese adult healthy subjects: a novel xanthine oxidase inhibitor topiroxostat was not associated with QT prolongation. J Clin Pharmacol. In press.
6 Giorgi MA, Bolaños R, Gonzalez CD, Di Girolamo G. QT interval prolongation: preclinical and clinical testing arrhythmogenesis in drugs and regulatory implications. Curr Drug Saf. 2010;5:54–57.
7 Chi KR. Revolution dawning in cardiotoxicity testing. Nat Rev Drug Discov. 2013;12:565–567.
8 Yamazaki K, Hihara T, Taniguchi T, Kohmura N, Yoshinaga T, Ito M, et al. A novel method of selecting human embryonic stem cell-derived cardiomyocyte clusters for assessment of potential to influence QT interval. Toxicol In Vitro. 2012;26:335–342.
9 He JQ, Ma Y, Lee Y, Thomson JA, Kamp TJ. Human embryonic stem cells develop into multiple types of cardiac myocytes: action potential characterization. Circ Res. 2003;93:32–39.
10 Itzhaki I, Maizels L, Huber I, Zwi-Dantsis L, Caspi O, Winterstern A, et al. Modelling the long QT syndrome with induced pluripotent stem cells. Nature. 2011;471:225–229.
11 Nalos L, Varkevisser R, Jonsson MK, Houtman MJ, Beekman JD, van der Nagel R, et al. Comparison of the I_{Kr} blockers moxifloxacin, dofetilide and E-4031 in five screening models of pro-arrhythmia reveals lack of specificity of isolated cardiomyocytes. Br J Pharmacol. 2012;165:467–478.
12 Schaaf S, Shibamiya A, Mewe M, Eder A, Stöhr A, Hirt MN, et al. Human engineered heart tissue as a versatile tool in basic research and preclinical toxicology. PLoS One. 2011;6:e26397.
13 Tanaka T, Tohyama S, Murata M, Nomura F, Kaneko T, Chen H, et al. In vitro pharmacologic testing using human induced pluripotent stem cell-derived cardiomyocytes. Biochem Biophys Res Commun. 2009;385:497–502.
14 Fridericia LS. Die sytolendauer in elektrokardiogramm bei normalen menshen und bei herzfranken. Acta Med Scand. 1920;53:469–486. (text in German)
15 Fujiki A, Tani M, Mizumaki K, Shimono M, Inoue H. Electrophysiologic effects of intravenous E-4031, a novel class III antiarrhythmic agent, in patients with supraventricular tachyarrhythmias. J Cardiovasc Pharmacol. 1994;23:374–378.
16 Verheijck EE, van Ginneken AC, Bourier J, Bouman LN. Effects of delayed rectifier current blockade by E-4031 on impulse generation in single sinoatrial nodal myocytes of the rabbit. Circ Res. 1995;76:607–615.
17 Brouillette J, Lupien MA, St-Michel C, Fiset C. Characterization of ventricular repolarization in male and female guinea pigs. J Mol Cell Cardiol. 2007;42:357–366.
18 Tabo M, Komatsu R, Isobe T, Honda M, Yamada Y, Kimura K. Accurate detection of drug-induced delayed ventricular repolarization with a suitable correction formula in Langendorff guinea pig heart. J Toxicol Sci. 2010;35:687–698.
19 Asano Y, Davidenko JM, Baxter WT, Gray RA, Jalife J. Optical mapping of drug-induced polymorphic arrhythmias and torsade de pointes in the isolated rabbit heart. J Am Coll Cardiol. 1997;29:831–842.
20 Maruyama M, Lin SF, Xie Y, Chua SK, Joung B, Han S, et al. Genesis of phase 3 early afterdepolarizations and triggered activity in acquired long-QT syndrome. Circ Arrhythm Electrophysiol. 2011;4:103–111.
21 Zhou Z, Gong Q, Ye B, Fan Z, Makielski JC, Robertson GA, et al. Properties of HERG channels stably expressed in HEK 293 cells studied at physiological temperature. Biophys J. 1998;74:230–241.
22 Sanguinetti MC, Jurkiewicz NK, Scott A, Siegl PK. Isoproterenol antagonizes prolongation of refractory period by the class III antiarrhythmic agent E-4031 in guinea pig myocytes. Mechanism of action. Circ Res. 1991;68:77–84.
23 Wettwer E, Scholtysik G, Schaad A, Himmel H, Ravens U. Effects of the new class III antiarrhythmic drug E-4031 on myocardial contractility and electrophysiological parameters. J Cardiovasc Pharmacol. 1991;17:480–487.
24 Omata T, Kasai C, Hashimoto M, Hombo T, Yamamoto K. QT PRODACT: comparison of non-clinical studies for drug-induced delay in ventricular repolarization and their role in safety evaluation in humans. J Pharmacol Sci. 2005;99:531–541.
25 Hashimoto K, Haruno A, Matsuzaki T, Hirasawa A, Awaji T, Uemura Y. Effects of a new class III antiarrhythmic drug (E-4031) on canine ventricular arrhythmia models. Asia Pac J Pharmacol. 1991;6:127–137.
26 Katritsis D, Morgan J, Brachmann J, Bygrave A, O'Farrell D, Rowland E, et al. Electrophysiological effects of E 4031, a drug with selective class III properties, in man. Pacing Clin Electrophysiol. 1997;20:930–937.

セッション2-2　ICH S7Bに関する今後の展望—新しいパラダイムの主な方向
(心臓安全性薬理学研究のためのiPS細胞由来心筋細胞)

ヒトiPS細胞を用いた成熟心筋細胞の開発

諫田泰成

Ⅰ．はじめに

ヒトiPS細胞の医療分野への応用として，大きく分けて「再生医療」と「創薬」があげられる[1]．再生医療への注目度は非常に高く，2013年にヒトiPS細胞から作製した網膜色素上皮細胞を移植する臨床研究が承認され，造腫瘍性など様々な観点から検証される予定である[2]．一方，創薬応用は，モデルとなる分化細胞を作製して*in vitro*のアッセイ系で使用するため，ウイルスなど様々な加工が可能であるが，医薬品の安全性や有効性を評価するためには，ヒト成体組織を反映した分化細胞が必要不可欠である．

ヒトiPS細胞は2007年の樹立から多くの知見が蓄積され，未分化ヒトiPS細胞には株間の差や継代数の差，研究室間における差などのバリエーションが存在することが明らかになり[3]，国際幹細胞イニシアティブなどによるプロジェクトにおいても標準化作業が進められているが，実用化において最も重要な分化細胞の標準化に関しては，思うように進んでいない．今後，分化誘導の標準プロトコールを整備して，分化細胞の品質基準などを定めることにより，実用化が加速すると思われる．

本稿では，ヒトiPS細胞から心筋細胞への分化誘導技術ならびに分化心筋細胞の薬理学的な特性を概説し，医薬品による催不整脈作用に対する応用可能性，さらにはICHガイドラインへの展望について議論したい．

Ⅱ．医薬品による催不整脈作用

医薬品によって発生する副作用の中で，torsade de pointes (TdP)とよばれる重篤な不整脈は重要である[4]．発生頻度は極めて少ないものの，心室細動に移行し突然死に至る症例が報告されている．TdPはQT間隔の延長を伴うことから，現在TdP誘発リスクは，非臨床試験として*in vitro*でカリウム電流(hERGチャネル)阻害作用を検討している．次いで*in vivo*で動物のQT延長作用を評価し，その後，臨床においてThorough QT/QTc試験により厳密にヒトのQT間隔に対する作用を調べることで，総合的にTdP誘発リスクを評価している．これらのガイドラインが整備された後は，薬剤性の心毒性に関して大きな問題は起きていないことから，一定の評価ができていると考えられる．しかしながら，hERG試験で有用な医薬品候補化合物を見落としてしまう可能性，TdP ≠ QT延長であること，hERG試験だけではわからない不整脈作用があることなど，問題点がいまだ残されている．iPS心筋細胞はヒトの細胞であり，さらにマルチチャネルを発現し

国立医薬品食品衛生研究所薬理部第二室

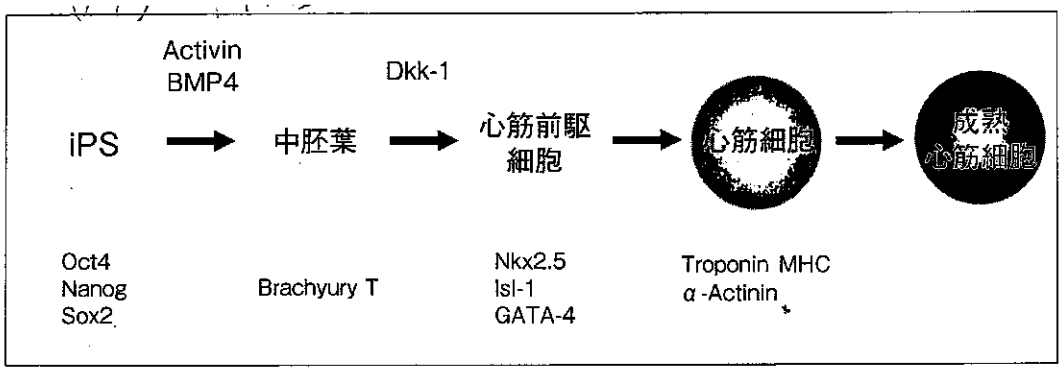

図1　ヒトiPS細胞から成熟心筋細胞の分化誘導法

ており総合的な評価が可能であることから[5]，hERG試験よりも予測性が向上するのではないか，と期待は大きい．

Ⅲ．ヒトiPS細胞を用いた心筋分化誘導法

ヒトiPS細胞の心筋分化誘導法は，EB形成法と定方向分化誘導法の2種類に大きく分類できる．ここでは，定方向分化誘導法に絞って述べる[6]．ヒトiPS細胞にサイトカインや増殖因子などを用いることにより，中胚葉，心筋前駆細胞，心筋細胞と段階的に分化誘導を行うことができる(図1)．具体的には，ヒトiPS細胞をマトリゲルでコートしたディッシュに高密度で播種して数日間培養をした後，ActivinとBMP-4により中胚葉へ分化誘導する．次に，Wnt antagonistであるDickkopf-1(Dkk-1)など，Wntシグナル修飾剤を用いて心筋前駆細胞に分化させる．さらに，心筋前駆細胞はVEGFなどの増殖因子の存在下で培養することにより，心筋細胞に分化して自律的な拍動が観察される．

このように作製されたiPS心筋細胞は，未成熟であると考えられている．パッチクランプにより電気生理学的特性を検討すると，静止膜電位は通常-90 mV程度であるのに対して，iPS心筋細胞はいずれも-50 mV程度と浅い．米国Cellular Dynamics International社(CDI)から販売されているiCell心筋細胞も同様の傾向を示したことから，元のiPS細胞株や分化誘導法に依存せず，iPS心筋細胞に共通の課題であると考えられる．

医薬品の作用を評価する上で，成熟した心筋が必要であるのかはわかっていない．すでに心筋の成熟化を促進するためのアプローチとして，電気刺激など様々な手法が検討されている[7]．われわれは成体心室筋と比較して，iPS心筋細胞において不足している因子に着目し，心筋細胞の成熟化を誘導できる方法を明らかにしている(論文投稿中)．われわれが検討した範囲では，アデノウイルスの感染効率は，未分化よりも分化が進んだiPS細胞のほうが高かったことから，iPS心筋細胞にアデノウイルスを用いて遺伝子導入することにより，成熟化を誘導している．図2の模式図に示したように，E-4031によるAPD延長は，成熟心筋細胞のほうが有用であるという予備的な結果を得ており(図2)，一定レベルの成熟した心筋細胞が必要であると考えられる．今後，薬剤評価用にさらなる改良を行い，予測性の高いモデルへと発展させたい．

Ⅳ．iPS心筋細胞を用いた薬理試験

薬理試験に用いる分化心筋細胞の形状としては，個々の細胞，EBなどの細胞塊，シート状の細胞などがあげられる．個々の細胞の場合は，パッチクランプで解析が可能である．一つ一つの細胞の活動電位の波形をもとにQT間隔を評価するため，心筋細胞のサブタイプの情報も同時に得られるが，スループット性は極めて低い．さらには，個々の細胞のばらつきの問題が残されている．

一方，細胞塊やシート状の標本に関しては，多点

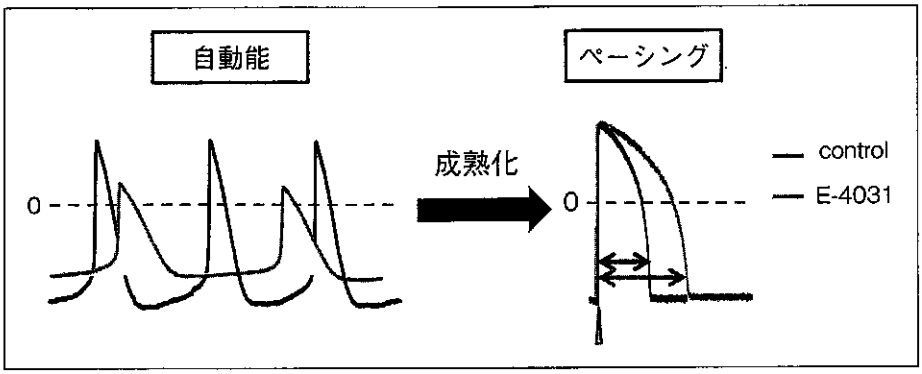

図2
成熟心筋細胞におけるE-4031の作用

電極システムを用いて，電極を埋め込んだディッシュに細胞塊やシートを接着させると，QT間隔に相当する細胞外電位(field potential：FP)の測定が可能である．個々の心筋細胞のばらつきが平均化されるため，比較的安定したデータが得られることが期待される．また，侵襲がないため，医薬品候補化合物の長時間曝露による薬理作用が調べられ，電気生理学特有の敷居の高さはなく，比較的簡便である．ただし，多点電極にしても，1日で解析できる数には限界があり，大規模なスクリーニングには向いていないので，改良が必要ではないかと思われる．

われわれは，iPS心筋細胞を用いた安全性薬理試験の確立を目指して，iCell心筋細胞をモデル細胞として用いて細胞外電位装置による評価を行った[8]．その結果，hERG阻害剤E-4031の添加により，濃度依存的にFP延長が観察された．さらに，E-4031により，triggered activityやEADなどの異常な波形を検出できることが明らかになった．こちらはFPD (FP duration)とは異なり，既存の *in vitro* 評価系では検出できないような不整脈のリスク評価につながると考えられ，非常に興味深い．現在，われわれは成熟した心筋細胞を用いて，同様の検討を行っている．

V．ガイドラインに向けて

上述のように，iPS心筋細胞を使った安全性薬理試験系が確立し，催不整脈作用の総合的な理解につながることが明らかになれば，ICHのガイドラインへの追加も期待される．そのためには，多くの陽性対照物質や陰性対照物質を用いて，多施設間で検証作業を行い，科学的根拠を得る必要がある．日本としても明確なデータを用意しなければならない．

このような背景の下，2013年7月から，FDA/HESI/CSRCにおいてCiPA (Comprehensive *in vitro* Proarrhythmia Assay)の枠組みが発足し，薬剤による不整脈誘発リスク評価に関する国際的な議論も開始された[9),10)]．この動きはヒトiPS細胞に限定されたわけではないが，ヒト幹細胞由来心筋細胞のワーキンググループが本格的に活動を開始しており，iPS心筋細胞への期待がうかがえる．CiPAの議論を受けて，現行のhERG阻害/QT延長に基づく催不整脈リスク評価ガイドライン(S7B)とTQT試験(E14)の改訂につながる可能性があり，今後，国際協調を図っていく必要がある．

VI．まとめ

ヒトiPS細胞の分化誘導技術などの研究が進展し，またCiPAなどの国際的な議論も開始されたことにより，iPS心筋細胞を心毒性試験に応用する機運が高まってきている．実用化に向けては，ヒトiPS細胞の元の株間の差，iPS心筋細胞の特性解析や大量かつ安定した供給体制の確立，安全性薬理評価法の開発などを，一つ一つ丹念に地道に検証する作業が不可欠である．また，多施設間による協力体制も必要不可欠である．将来的には，日本発のヒトiPS細胞技術を用いて心毒性の発生を回避すること

が可能となり，より安全な医薬品が提供されることを期待したい．

謝　辞

本研究は，国立医薬品食品衛生研究所薬理部 関野祐子先生，東京医科歯科大学難治疾患研究所生体情報薬理学分野 古川哲史先生，黒川洵子先生，滋賀医科大学 芦原貴司先生との共同研究であり，代表して執筆させていただきました．心より深く感謝申し上げます．

また，東邦大学医学部薬理学講座 杉山篤先生，安東賢太郎先生，中村裕二先生，エーザイ株式会社 澤田光平先生，宮本憲優先生，株式会社新日本科学 松尾純子先生に的確なご教示とご指導を賜りましたことに心より御礼申し上げます．

〔文　献〕

1）Grskovic M, Javaherian A, Strulovici B, Daley GQ : Induced pluripotent stem cells--opportunities for disease modelling and drug discovery. Nat Rev Drug Discov, 2011 ; 10 : 915～929
2）Kuroda T, Yasuda S, Kusakawa S, Hirata N, Kanda Y, Suzuki K, Takahashi M, Nishikawa S, Kawamata S, Sato Y : Highly sensitive in vitro methods for detection of residual undifferentiated cells in retinal pigment epithelial cells derived from human iPS cells. PLoS One, 2012 ; 7 : e37342
3.) Bock C, Kiskinis E, Verstappen G, Gu H, Boulting G, Smith ZD, Ziller M, Croft GF, Amoroso MW, Oakley DH, Gnirke A, Eggan K, Meissner A : Reference Maps of human ES and iPS cell variation enable high-throughput characterization of pluripotent cell lines. Cell, 2011 ; 144 : 439～452
4）Ferri N, Siegl P, Corsini A, Herrmann J, Lerman A, Benghozi R : Drug attrition during pre-clinical and clinical development : understanding and managing drug-induced cardiotoxicity. Pharmacol Ther, 2013 ; 138 : 470～484
5）Burridge PW, Keller G, Gold JD, Wu JC : Production of de novo cardiomyocytes : human pluripotent stem cell differentiation and direct reprogramming. Cell Stem Cell, 2012 ; 10 : 16～28
6）Uosaki H, Fukushima H, Takeuchi A, Matsuoka S, Nakatsuji N, Yamanaka S, Yamashita JK : Efficient and scalable purification of cardiomyocytes from human embryonic and induced pluripotent stem cells by VCAM1 surface expression. PLoS ONE, 2011 ; 6 : e23657
7）Lieu DK, Fu JD, Chiamvimonvat N, Tung KC, McNerney GP, Huser T, Keller G, Kong CW, Li RA : Mechanism-based facilitated maturation of human pluripotent stem cell-derived cardiomyocytes. Circ Arrhythm Electrophysiol, 2013 ; 6 : 191～201
8）Nakamura Y, Matsuo J, Miyamoto N, Ojima A, Ando K, Kanda Y, Sawada K, Sugiyama A, Sekino Y : Assessment of testing methods for drug-induced repolarization delay and arrhythmias in an iPS cell-derived cardiomyocyte sheet : multi-site validation study. J Pharmacol Sci, 2014 ; 124 : 494～501
9）Chi KR : Revolution dawning in cardiotoxicity testing. Nat Rev Drug Discov, 2013 ; 12 : 565～567
10) Sager PT, Gintant G, Turner JR, Pettit S, Stockbridge N : Rechanneling the cardiac proarrhythmia safety paradigm : a meeting report from the Cardiac Safety Research Consortium. Am Heart J, 2014 ; 167 : 292～300

Metallomics

PAPER

View Article Online
View Journal

Cite this: DOI: 10.1039/c5mt00033e

Tributyltin induces mitochondrial fission through NAD-IDH dependent mitofusin degradation in human embryonic carcinoma cells

Shigeru Yamada,[a] Yaichiro Kotake,[b] Mizuho Nakano,[a] Yuko Sekino[a] and Yasunari Kanda*[a]

Received 4th February 2015,
Accepted 14th April 2015

DOI: 10.1039/c5mt00033e

www.rsc.org/metallomics

Organotin compounds, such as tributyltin (TBT), are well-known endocrine disruptors. TBT acts at the nanomolar level through genomic pathways *via* the peroxisome proliferator activated receptor (PPAR)/retinoid X receptor (RXR). We recently reported that TBT inhibits cell growth and the ATP content in the human embryonic carcinoma cell line NT2/D1 *via* a non-genomic pathway involving NAD^+-dependent isocitrate dehydrogenase (NAD-IDH), which metabolizes isocitrate to α-ketoglutarate. However, the molecular mechanisms by which NAD-IDH mediates TBT toxicity remain unclear. In the present study, we evaluated the effects of TBT on mitochondrial NAD-IDH and energy production. Staining with MitoTracker revealed that nanomolar TBT levels induced mitochondrial fragmentation. TBT also degraded the mitochondrial fusion proteins, mitofusins 1 and 2. Interestingly, apigenin, an inhibitor of NAD-IDH, mimicked the effects of TBT. Incubation with an α-ketoglutarate analogue partially recovered TBT-induced mitochondrial dysfunction, supporting the involvement of NAD-IDH. Our data suggest that nanomolar TBT levels impair mitochondrial quality control *via* NAD-IDH in NT2/D1 cells. Thus, mitochondrial function in embryonic cells could be used to assess cytotoxicity associated with metal exposure.

Introduction

Growing evidence suggests that environmental organometals contribute to the observed increase in neurodevelopmental disorders, such as learning disabilities, autism spectrum disorder, behavioral abnormalities and teratogenicity.[1–3] Since the developing brain is more vulnerable to injury than the adult brain, exposure to these organometals during early fetal development can cause permanent or delayed neural disorders at much lower doses than in adults.[4–7] Therefore, it is necessary to elucidate the cytotoxic effects of organometals at low levels during development.

Organotin compounds, such as TBT, are well known to cause various types of cytotoxicity *via* genomic and non-genomic pathways. In the genomic pathway, nanomolar concentrations of TBT activate the retinoid X receptor (RXR) and/or peroxisome proliferator-activated receptor γ (PPARγ) and result in neurodevelopmental defects in mammals.[8,9] Conversely, many reports have shown that TBT at micromolar levels causes mitochondorial toxicity in the non-genomic pathway. For example, micromolar TBT and dibutyltin (DBT) levels have been shown to prevent mitochondrial respiration by inhibiting the electron transfer from complexes I and III, and Mg-ATPase activity.[10–12] The non-genomic effect of TBT mediates cell death in rat neurons. TBT induces neuronal death *via* AMPK activation and the phosphorylation of the mammalian target of rapamycin (mTOR) in rat cortical neurons.[13,14] TBT also induces neuronal degeneration *via* mitochondria-mediated ROS generation in rat neurons.[15]

We studied nanomolar TBT toxicity using neuronal precursor NT2/D1 cells as a model of the neurodevelopmental stage[16] and found that nanomolar TBT levels inhibit intracellular energy metabolism, including ATP production, *via* mitochondrial NAD^+-dependent isocitrate dehydrogenase (NAD-IDH), which catalyzes the irreversible conversion of isocitrate to α-ketoglutarate in the tricarboxylic acid (TCA) cycle.[17,18] Based on these observations, we hypothesized that nanomolar TBT levels affect mitochondrial functions, thereby altering the energy metabolism of neuronal precursor cells.[19]

Mitochondria continuously change their morphology through fission and fusion. These mitochondrial dynamics are an important quality control mechanism that maintains mitochondrial function, such as ATP production.[20] Mitochondrial fission and fusion are regulated by several GTPases. In mitochondrial fusion, mitofusins 1 and 2 (Mfn1, 2) and optic atrophy 1 (Opa1) induce the fusion of the outer and inner mitochondrial membranes,

[a] *Division of Pharmacology, National Institute of Health Sciences, 1-18-1, Kamiyoga, Setagaya-ku 158-8501, Japan. E-mail: kanda@nihs.go.jp; Fax: +81-3-3700-9704; Tel: +81-3-3700-9704*

[b] *Department of Xenobiotic Metabolism and Molecular Toxicology, Graduate School of Biomedical and Health Sciences, Hiroshima University, Japan*

respectively.[21,22] The deletion of Mfn1 and Mfn2 in mice is embryonically lethal, and cells from these embryos contain fragmented and dysfunctional mitochondria.[23] In contrast, dynamin-related protein 1 (Drp1) is a cytoplasmic protein that assembles into rings surrounding the outer mitochondrial membrane, where it interacts with fission protein 1 (Fis1) to promote fission.[24,25]

In the present study, we have investigated the effect of TBT on mitochondrial quality control in NT2/D1 cells. We found that exposure to 100 nM TBT induced proteasomal degradation of Mfn and mitochondrial fragmentation through an NAD-IDH-dependent mechanism. Thus, impaired mitochondrial quality control is a novel mechanism of nanomolar level TBT-induced toxicity in human embryonic carcinoma cells.

Methods

Cell culture

NT2/D1 cells were obtained from the American Type Culture Collection (Manassas, VA, USA). The cells were cultured in Dulbecco's modified Eagle's medium (DMEM; Sigma-Aldrich, St Louis, MO, USA) supplemented with 10% fetal bovine serum (FBS; Biological Industries, Ashrat, Israel) and 0.05 mg ml^{-1} of the penicillin–streptomycin mixture (Life Technologies, Carlsbad, CA, USA) at 37 °C in 5% CO_2.

Assessment of mitochondrial fusion

After treatment with TBT (100 nM, 24 h), the cells were fixed with 4% paraformaldehyde and stained with 50 nM Mito-Tracker Red CMXRos (Cell Signaling Technology, Danvers, MA, USA) and 0.1 μg ml^{-1} 4′,6-diamidino-2-phenylindole (DAPI; Dojin, Kumamoto, Japan). Changes in the mitochondrial morphology were observed using confocal laser microscopy (Nicon A1). Images (n = 3–7) of random fields were obtained, and the number of cells displaying mitochondrial fusion (<10% punctiform) was counted in each image, as previously reported.[26]

Real-time PCR

Total RNA was isolated from NT2/D1 cells using the TRIzol reagent (Life Technologies), and quantitative real-time reverse transcription (RT)-PCR using a QuantiTect SYBR Green RT-PCR Kit (QIAGEN, Valencia, CA, USA) was performed using an ABI PRISM 7900HT sequence detection system (Applied Biosystems, Foster City, CA, USA), as previously reported.[27] The relative change in the amount of transcript was normalized to the mRNA levels of glyceraldehyde-3-phosphate dehydrogenase (GAPDH). The following primer sequences were used for real-time PCR analysis: human Drp1: forward, 5-TGGGCGCCGACATCA-3, reverse, 5-GCT CTGCGTTCCCACTACGA-3; human Fis1: forward, 5-TACGTCCG CGGGTTGCT-3, reverse, 5-CCAGTTCCTTGGCCTGGTT-3; human Mfn1: forward, 5-GGCATCTGTGGCCGAGTT-3, reverse, 5-ATTAT GCTAAGTCTCCGCTCCAA-3; human Mfn2: forward, 5-GCTCG GAGGCACATGAAAGT-3, reverse, 5-ATCACGGTGCTCTTCCCATT-3; human GAPDH: forward, 5-GTCTCCTCTGACTTCAACAGCG-3, reverse, 5-ACCACCCTGTTGCTGTAGCCAA-3.

Western blot analysis

Western blot analysis was performed as previously reported.[28] Briefly, the cells were lysed with cell lysis buffer (Cell Signaling Technology). The proteins were then separated by sodium dodecyl sulfate-polyacrylamide gel electrophoresis (SDS-PAGE) and electrophoretically transferred to Immobilon-P (Millipore, Billerica, MA, USA). The membranes were probed using the following antibodies: an anti-Mfn1 polyclonal antibody (1 : 1000; Cell Signaling Technology), an anti-Mfn2 monoclonal antibody (1 : 1000; Cell Signaling Technology), an anti-cytochrome c oxidase subunit IV (COX IV) monoclonal antibody (1 : 1000; Cell Signaling Technology), and an anti-β-actin monoclonal antibody (1 : 5000; Sigma-Aldrich). The membranes were then incubated with secondary antibodies against rabbit or mouse IgG conjugated to horseradish peroxidase (Cell Signaling Technology). The bands were visualized using the ECL western blotting analysis system (GE Healthcare, Buckinghamshire, UK), and images were acquired using a LAS-3000 imager (FUJIFILM UK Ltd., Systems, Bedford, UK).

Chemicals and reagents

Tributyltin chloride was obtained from Tokyo Chemical Industry (Tokyo, Japan). Tin acetate (TA), rosiglitazone (RGZ), CD3254,

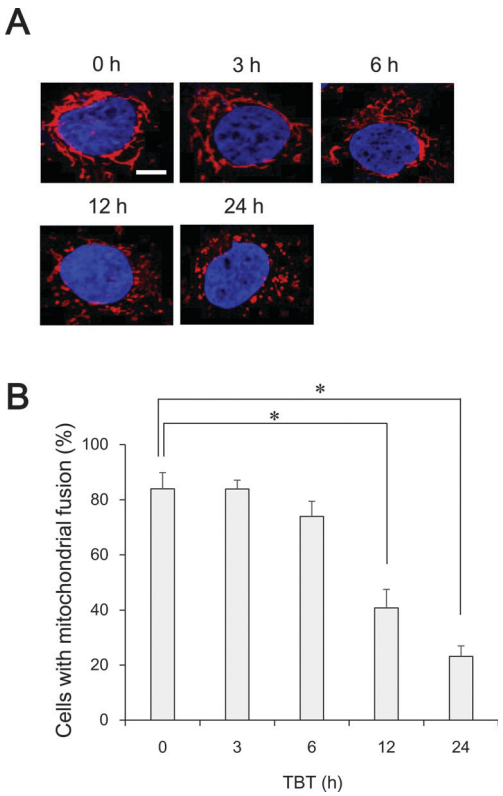

Fig. 1 Effect of TBT on the mitochondrial morphology in NT2/D1 cells. Cells were exposed to 100 nM TBT for 3, 6, 12, or 24 h. (A) The cells were stained with MitoTracker Red CMXRos and DAPI. Mitochondrial morphology was observed by confocal laser microscopy. Bar = 10 μm. (B) The number of cells undergoing mitochondrial fusion (<10% punctiform) was counted in each image. Data represent mean ± s.d. (n = 5). *P < 0.05.

apigenin, cycloheximide (CHX), carbonylcyanide m-chlorophenylhydrazone (CCCP), and MG132 were obtained from Sigma-Aldrich.

Statistical analysis

All data were presented as means ± S.D. ANOVA followed by a *post hoc* Tukey' test was used to analyze data in Fig. 1B, 2B, 3C, 4C, 5B, and 5C. Student's *t*-test was used to analyze data in Fig. 3A and 4B. *P*-values less than 0.05 were considered to be statistically significant.

Results and discussion

Effects of TBT on mitochondrial morphology

We have previously examined the effect of TBT (30–300 nM) on cell growth in NT2/D1 cells and found that TBT levels at the concentrations of 100 nM or more induced growth arrest in the cells.[17] Here we investigated whether 100 nM TBT affects mitochondrial dynamics in the cells. After exposure to 100 nM TBT for 12 h, we observed the increase in the number of cells with fragmented mitochondria, as compared to untreated control cells (Fig. 1A, B). After 24 h, the proportion of cells with mitochondrial fusion was nearly 80%. As a positive control, we used CCCP, which induces mitochondrial uncoupling and mitochondrial fission in other cells.[29] As expected, fragmented mitochondria were also observed following CCCP treatment for 24 h (Fig. 2A and B). In contrast, exposure to tin acetate (TA), which is less toxic, did not affect the mitochondrial morphology. To investigate whether TBT-induced mitochondrial fission was caused by changes in transcription, we treated the cells with the protein synthesis inhibitor cycloheximide. Treatment with cycloheximide did not alter the effects of TBT on the mitochondrial morphology (Fig. 2A and B). Moreover, rosiglitazone, an agonist of the TBT genomic target PPARγ, did not induce mitochondrial fragmentation. These results suggest that TBT induces mitochondrial fission through a non-genomic pathway in NT2/D1 cells.

TBT exposure induces proteasomal degradation of Mfn1 and 2

To examine the molecular mechanism by which TBT induces mitochondrial fragmentation, we assessed the effect of TBT on

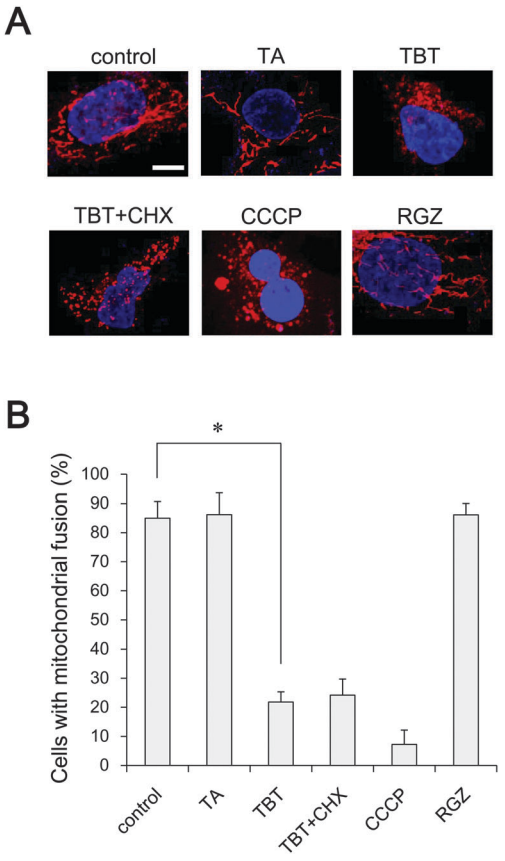

Fig. 2 Non-genomic effect of TBT-induced mitochondrial fission. Cells were exposed to 100 nM TA, 100 nM TBT, 100 nM TBT + 10 μg ml^{-1} cycloheximide (CHX), 1 μM CCCP or 100 nM rosiglitazone (RGZ) for 24 h. (A) The cells were stained with MitoTracker Red CMXRos and DAPI. Mitochondrial morphology was observed by confocal laser microscopy. Bar = 10 μm. (B) The number of cells undergoing mitochondrial fusion (<10% punctiform) was counted in each image. Data represent mean ± s.d. (n = 5). *P < 0.05.

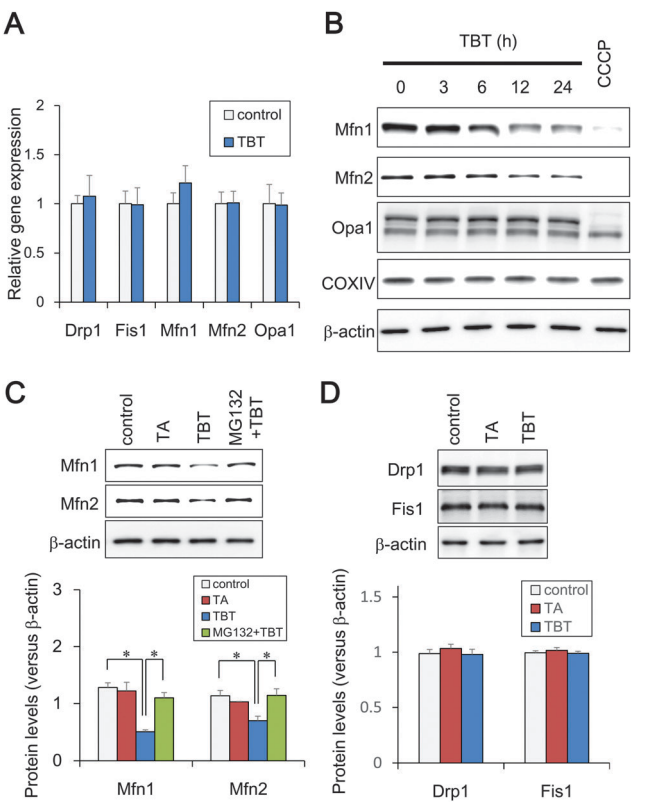

Fig. 3 Effect of TBT on mitochondrial protein levels in NT2/D1 cells. (A) After 24 h TBT exposure, the expression of mitochondrial genes was analyzed by real time PCR. The gene expression was not significantly altered by TBT exposure. (B) After TBT exposure for 3, 6, 12, or 24 h, mitochondrial proteins were analyzed by western blot using anti-Mfn1, Mfn2, Opa1, COXIV, or β-actin antibodies. (C) Cells were exposed to 100 nM TA, 100 nM TBT, or 100 nM TBT + 3 μM MG132 for 6 h. Mitochondrial proteins were analyzed by western blot using anti-Mfn1 or Mfn2 antibodies. (D) After 6 h TBT exposure, other mitochondrial proteins were analyzed by western blot using anti-Drp1, Fis1, or β-actin antibodies. Data represent mean ± s.d. (n = 3). *P < 0.05.

mitochondrial fission (Fis1, Drp1) and fusion genes (Mfn1, Mfn2, OPA1). Real-time PCR analysis showed that each gene expression was not significantly altered by TBT exposure (Fig. 3A). Fusion allows damaged mitochondria to incorporate into intact mitochondria, thereby maintaining mitochondrial function.[30] Dysfunctional mitochondria may lose their fusion capacity by the degradation of fusion proteins, resulting in the accumulation of fragmented mitochondria. Thus, we assessed the protein expression of Mfn1, Mfn2, and OPA1 in the presence or absence of TBT. Western blot analysis revealed that Mfn1 and Mfn2 protein levels were significantly reduced after 6 h, whereas OPA1 protein expression was not changed after 24 h (Fig. 3B and C). The other mitochondrial inner membrane protein, cytochrome *c* oxidase subunit IV (COX IV), was also not changed after 24 h (Fig. 3B). Moreover, MG132, a proteasome inhibitor, recovered the TBT-induced reduction in Mfn1 and Mfn2 (Fig. 3C). In contrast, the fusion proteins Fis1 and Drp1 were not affected by TBT (Fig. 3D). These data suggest that TBT-induced mitochondrial fragmentation is caused by the proteasomal degradation of Mfn1 and Mfn2.

Consistent with our data, chemical stressors have been reported to cause mitochondrial fission through the proteasomal degradation of Mfn. For example, doxorubicin induces ubiquitin-mediated proteasomal degradation of Mfn2, which facilitates mitochondrial fragmentation and apoptosis in sarcoma U2OS cells.[31] Another study has shown that CGP37157, an inhibitor of mitochondrial calcium efflux, mediates mitochondrial fission through Mfn1 degradation *via* ubiquitin ligase in prostate cancer LNCaP cells.[32] Since it remains unknown if ubiquitin ligases are involved or not in these TBT actions, further studies should be addressed to clarify the TBT-induced mechanism of proteasomal degradation of Mfn1 and Mfn2.

TBT induces mitochondrial defects *via* NAD-IDH

To investigate whether Mfn degradation and mitochondrial dysfunction are mediated through the non-genomic TBT target NAD-IDH, we examined the effects of apigenin, an NAD-IDH inhibitor,[33] on mitochondrial function. Apigenin (10 μM) decreased the number of cells undergoing mitochondrial fusion and induced mitochondrial fragmentation after 24 h (Fig. 4A and B). Furthermore, apigenin significantly reduced Mfn1 and Mfn2 protein expression, which was recovered by MG132 treatment (Fig. 4C). Apigenin has been reported to inhibit not only NAD-IDH but also hnRNPA2 and NF-κB.[33]

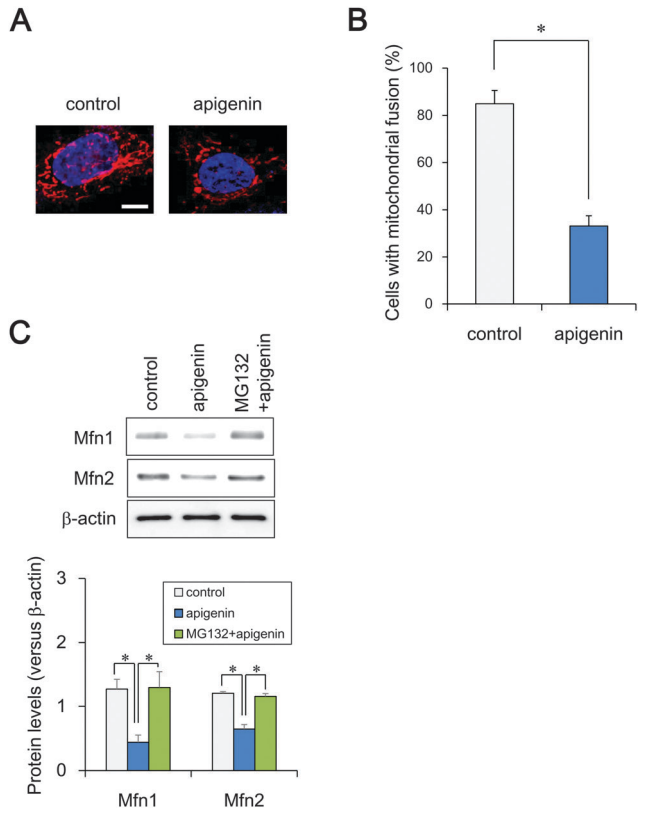

Fig. 4 Effect of apigenin on mitochondrial function in NT2/D1 cells. Cells were exposed to 10 μM apigenin. (A) Cells were stained with MitoTracker Red CMXRos and DAPI. Mitochondrial morphology was observed by confocal laser microscopy. Bar = 10 μm. (B) The number of cells undergoing mitochondrial fusion (<10% punctiform) was counted in each image. Data represent mean ± s.d. (n = 5). (C) Mitochondrial proteins in the cell lysate were analyzed by western blotting using anti-Mfn1 or Mfn2 antibodies. Data represent mean ± s.d. (n = 3). *P < 0.05.

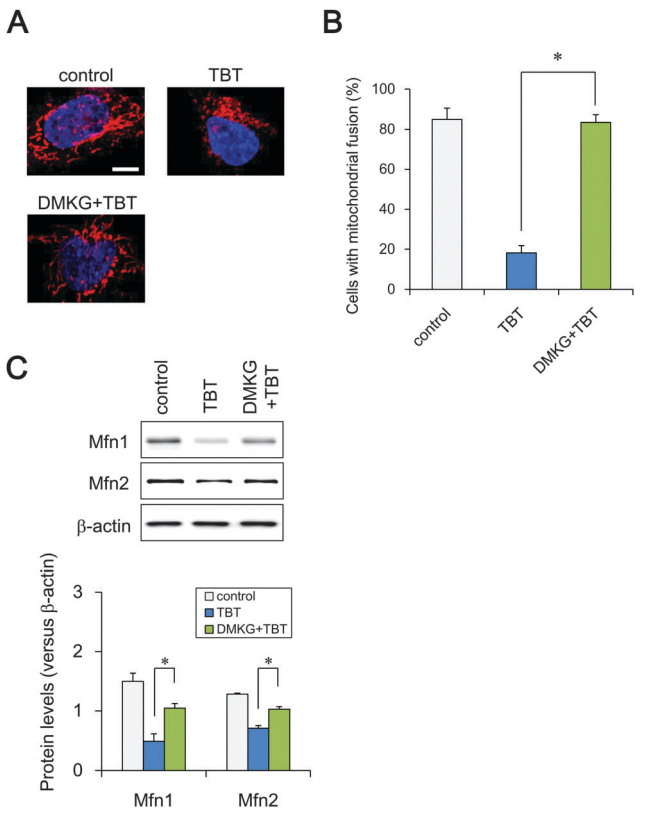

Fig. 5 Effect of DMKG on TBT-induced mitochondrial dysfunctions in NT2/D1 cells. Cells were exposed to 100 nM TBT and 7 mM DMKG. (A) Cells were stained with MitoTracker Red CMXRos and DAPI. Mitochondrial morphology was observed by confocal laser microscopy. Bar = 10 μm. (B) The number of cells undergoing mitochondrial fusion (<10% punctiform) was counted in each image. Data represent mean ± s.d. (n = 5). (C) Mitochondrial proteins were analyzed by western blotting using anti-Mfn1 or Mfn2 antibodies. Data represent mean ± s.d. (n = 3). *P < 0.05.

We cannot rule out the possibility that apigenin-induced mitochondrial dysfunction was induced by other targets. It is necessary to confirm our data by shRNA against NAD-IDH. To further confirm the involvement of NAD-IDH, we used dimethyl α-ketoglutarate (DMKG), a cell-permeable analog of α-ketoglutarate.[34] Incubation with DMKG prevented TBT-induced mitochondrial fragmentation in NT2/D1 cells (Fig. 5A) and recovered the number of cells undergoing mitochondrial fusion to the basal level (Fig. 5B). Furthermore, DMKG significantly recovered the TBT-induced the proteasomal degradation of Mfn1 and Mfn2 (Fig. 5C). Taken together, these data suggest that NAD-IDH mediates TBT-induced mitochondrial dysfunction *via* Mfn degradation in NT2/D1 cells. In addition to NAD-IDH, citrate synthase and α-ketoglutarate dehydrogenase also work as rate-limiting enzymes in the TCA cycle. Aluminium has been shown to induce oxidative stress *via* the negative regulation of citrate synthase and α-ketoglutarate dehydrogenase.[35,36] We could not rule out the possibility that TBT affects these enzymes. Several reports indicate that knockdown of Mfn1 and Mfn2 in the cells induces mitochondrial fragmentation and shows severe cellular defects, including decreased ATP content and poor cell growth.[30,37] Especially, Mfn2 has been reported to be necessary for striatal axonal projections of midbrain dopamine neurons by studies using dopamine neuron-specific Mfn2 knockout mice.[38] Taken together, Mfn1 and Mfn2 might be involved in several TBT actions *via* NAD-IDH, such as the reduction of ATP content, growth inhibition and enhancement of neuronal differentiation.

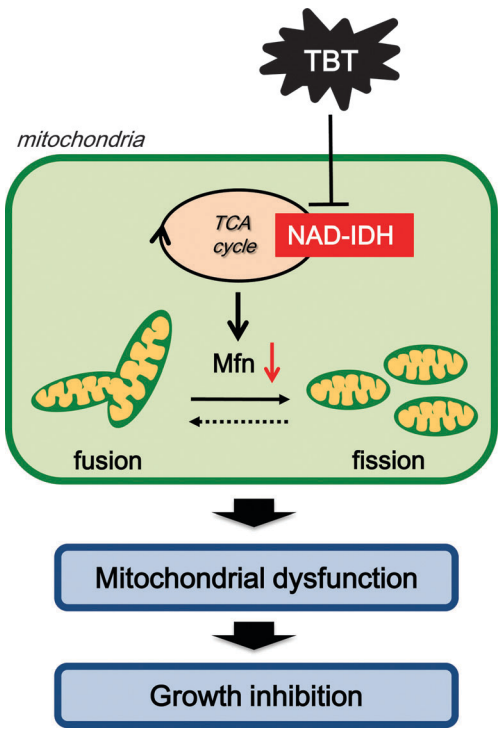

Fig. 6 Proposed model of TBT toxicity through non-genomic pathways in human embryonic carcinoma cells. Nanomolar TBT levels induce Mfn degradation and mitochondrial fission through NAD-IDH inhibition. These negative effects of TBT on mitochondrial quality control could mediate cell growth inhibition.

Conclusions

Based on our data, we have proposed a model of nanomolar TBT-induced mitochondrial dysfunction in neuronal precursor cells (Fig. 6). We demonstrated that TBT mediates the inhibition of NAD-IDH and the loss of mitochondrial quality control, representing a novel non-genomic pathway of TBT-induced toxicity. These negative effects of TBT on mitochondria could inhibit ATP production and cell growth. Since TBT at micromolar levels is known to cause neuronal degeneration *via* multiple mitochondrial defects, similar mitochondrial dysfunction might be also observed in immature neuronal precursor cells. We have previously revealed TBT-induced NAD-IDH inhibition in the rat brain. It would be interesting to study whether TBT-induced mitochondrial dysfunction *via* NAD-IDH might be also observed *in vivo*. We are now conducting experiments to determine how TBT degrades Mfn proteins both *in vitro* and *in vivo*. It remains to be determined if micromolar concentrations of TBT induce other mitochondrial dysfunctions in NT2/D1 cells and if the mechanisms pointed out here are selective for immature cells.

List of abbreviations

CCCP	Carbonylcyanide *m*-chlorophenylhydrazone
CHX	Cycloheximide
COX IV	Cytochrome *c* oxidase subunit IV
DAPI	4′,6-Diamidino-2-phenylindole
DMEM	Dulbecco's modified Eagle's medium
DMKG	Dimethyl α-ketoglutarate
Drp1	Dynamin-related protein 1
FBS	Fetal bovine serum
Fis1	Fission protein 1
GAPDH	Glyceraldehyde-3-phosphate dehydrogenase
Mfn	Mitofusin
NAD-IDH	NAD^+-dependent isocitrate dehydrogenase
Opa1	Optic atrophy 1
PPAR	Peroxisome proliferator activated receptor
RGZ	Rosiglitazone
RXR	Retinoid X receptor
TA	Tin acetate
TBT	Tributyltin
TCA	Tricarboxylic acid

Conflict of interest

The authors declare that there are no conflicts of interest.

Acknowledgements

This work was supported by a Health and Labour Sciences research grant from the Ministry of Health, Labour and Welfare, Japan (#H25-Kagaku-Ippan-002 to Y.Ka.), a grant-in-aid for scientific research from the Ministry of Education, Culture, Sports, Science, and Technology, Japan (#26293056, #26670041 to Y. Kanda), and a grant from the Smoking Research Foundation (Y. Kanda).

References

1 E. Dopp, L. M. Hartmann, A. M. Florea, A. W. Rettenmeier and A. V. Hirner, Environmental distribution, analysis, and toxicity of organometal(loid) compounds, *Crit. Rev. Toxicol.*, 2004, **34**, 301–333.

2 A. T. Gardlund, T. Archer, K. Danielsen, B. Danielsson, A. Frederiksson, N. G. Lindquist, H. Lindstrom and J. Luthman, Effects of prenatal exposure to tributyltin and trihexyltin on behavior in rats, *Neurotoxicol. Teratol.*, 1991, **13**, 99–105.

3 A. Mariani, R. Fanelli, A. Re Depaolini and M. De Paola, Decabrominated diphenyl ether and methylmercury impair fetal nervous system development in mice at documented human exposure levels, *Dev. Neurobiol.*, 2015, **75**, 23–38.

4 G. Winneke, Developmental aspects of environmental neurotoxicology: lessons from lead and polychlorinated biphenyls, *J. Neurol. Sci.*, 2011, **308**, 9–15.

5 L. G. Costa, M. Aschne, A. Vitalone, T. Syversen and O. P. Soldin, Developmental neuropathology of environmental agents, *Annu. Rev. Pharmacol. Toxicol.*, 2004, **44**, 87–110.

6 J. Dobbing, Vulnerable periods in developing brain, in *Appl. Neurochem*, ed. A. N. Davison and J. Dobbing, Davis, Philadelphia, 1968, pp. 287–316.

7 P. M. Rodier, Developing brain as a target of toxicity, *Environ. Health Perspect.*, 1995, **103**(suppl 6), 73–76.

8 T. Kanayama, N. Kobayashi, S. Mamiya, T. Nakanishi and J. Nishikawa, Organotin compounds promote adipocyte differentiation as agonists of the peroxisome proliferator-activated receptor gamma/retinoid X receptor pathway, *Mol. Pharmacol.*, 2005, **67**, 766–774.

9 M. Kajta and A. K. Wójtowicz, Impact of endocrine-disrupting chemicals on neural development and the onset of neurological disorders, *Pharmacol. Rep.*, 2013, **65**, 1632–1639.

10 H. S. Elsabbagh, S. Z. Moussa and O. S. El-tawil, Neurotoxicologic sequelae of tributyltin intoxication in rats, *Pharmacol. Res.*, 2002, **45**, 201–206.

11 S. Nesci, V. Ventrella, F. Trombetti, M. Pirini and A. Pagliarani, Tributyltin (TBT) and mitochondrial respiration in mussel digestive gland, *Toxicol. in Vitro*, 2011, **25**, 951–959.

12 S. Nesci, V. Ventrella, F. Trombetti, M. Pirini, A. R. Borgatti and A. Pagliarani, Tributyltin (TBT) and dibutyltin (DBT) differently inhibit the mitochondrial Mg-ATPase activity in mussel digestive gland, *Toxicol. in Vitro*, 2011, **25**, 117–124.

13 Y. Nakatsu, Y. Kotake, N. Takai and S. Ohta, Involvement of autophagy *via* mammalian target of rapamycin (mTOR) inhibition in tributyltin-induced neuronal cell death, *J. Toxicol. Sci.*, 2010, **35**, 245–251.

14 Y. Kotake, Molecular mechanisms of environmental organotin toxicity in mammals, *Biol. Pharm. Bull.*, 2012, **35**, 1876–1880.

15 S. Mitra, R. Gera, W. A. Siddiqui and S. Khandelwal, Tributyltin induces oxidative damage, inflammation and apoptosis *via* disturbance in blood–brain barrier and metal homeostasis in cerebral cortex of rat brain: an *in vivo* and *in vitro* study, *Toxicology*, 2013, **310**, 39–52.

16 M. Bani-Yaghoub, J. M. Felker and C. C. Naus, Human NT2/D1 cells differentiate into functional astrocytes, *NeuroReport*, 1999, **10**, 3843–3846.

17 S. Yamada, Y. Kotake, Y. Sekino and Y. Kanda, AMP-activated protein kinase-mediated glucose transport as a novel target of tributyltin in human embryonic carcinoma cells, *Metallomics*, 2013, **5**, 484–491.

18 S. Yamada, Y. Kotake, Y. Demizu, M. Kurihara, Y. Sekino and Y. Kanda, NAD-dependent isocitrate dehydrogenase as a novel target of tributyltin in human embryonic carcinoma cells, *Sci. Rep.*, 2014, **4**, 5952.

19 C. M. Nasrallah and T. L. Horvath, Mitochondrial dynamics in the central regulation of metabolism, *Nat. Rev. Endocrinol.*, 2014, **10**, 650–658.

20 R. J. Youle and A. M. van der Bliek, Mitochondrial fission, fusion, and stress, *Science*, 2012, **337**, 1062–1065.

21 T. Koshiba, S. A. Detmer, J. T. Kaiser, H. Chen, J. M. McCaffery and D. C. Chan, Structural basis of mitochondrial tethering by mitofusin complexes, *Science*, 2004, **305**, 858–862.

22 S. Cipolat, O. M. De Brito, B. Dal Zilio and L. Scorrano, OPA1 requires mitofusin 1 to promote mitochondrial fusion, *Proc. Natl. Acad. Sci. U. S. A.*, 2004, **101**, 15927–15932.

23 H. Chen, S. A. Detmer, A. J. Ewald, E. Erik, S. E. F. Griffin and D. C. Chan, Mitofusins mfn1 and mfn2 coordinately regulate mitochondrial fusion and are essential for embryonic development, *J. Cell Biol.*, 2003, **160**, 189–200.

24 E. Smirnova, L. Griparic, D.-L. Shurland and A. M. van der Bliek, Dynamin-related protein Drp1 is required for mitochondrial division in mammalian cells, *Mol. Biol. Cell*, 2001, **12**, 2245–2256.

25 Y. Yoon, E. W. Krueger, B. J. Oswald and M. A. McNiven, The mitochondrial protein hFis1 regulates mitochondrial fission in mammalian cells through an interaction with the dynamin-like protein DLP1, *Mol. Biol. Cell*, 2003, **23**, 5409–5420.

26 X. Fan, R. Hussien and G. A. Brooks, H_2O_2-induced mitochondrial fragmentation in C2C12 myocytes, *Free Radical Biol. Med.*, 2010, **49**, 1646–1654.

27 N. Hiarta, S. Yamada, T. Shoda, M. Kurihara, Y. Sekino and Y. Kanda, Sphingosine-1-phosphate promotes expansion of cancer stem cells *via* S1PR3 by a ligand-independent Notch activation, *Nat. Commun.*, 2014, **5**, 4806.

28 Y. Kanda, T. Hinara, S. W. Kang and Y. Watanabe, Reactive oxygen species mediate adipocyte differentiation in mesenchymal stem cells, *Life Sci.*, 2011, **89**, 250–258.

29 A. Tanaka, M. M. Cleland, S. Xu, D. P. Narendra, D. F. Suen, M. Karbowski and R. J. Youle, Proteasome and p97 mediate mitophagy and degradation of mitofusins induced by Parkin, *J. Cell Biol.*, 2010, **191**, 1367–1380.

30 H. Chen, A. Chomyn and D. C. Chan, Disruption of fusion results in mitochondrial heterogeneity and dysfunction, *J. Biol. Chem.*, 2005, **280**, 26185–26192.

31 G. P. Leboucher, Y. C. Tsai, M. Yang, K. C. Shaw, M. Zhou, T. D. Veenstra, M. H. Glickman and A. M. Weissman, Stress-induced phosphorylation and proteasomal degradation of mitofusin 2 facilitates mitochondrial fragmentation and apoptosis, *Mol. Cell*, 2012, **47**, 547–557.

32 V. Choudhary, I. Kaddour-Djebbar, R. Alaisami, M. V. Kumar and W. B. Bollag, Mitofusin 1 degradation is induced by a disruptor of mitochondrial calcium homeostasis, CGP37157: a role in apoptosis in prostate cancer cells, *Int. J. Oncol.*, 2014, **44**, 1767–1773.

33 D. Arango, K. Morohashi, A. Yilmaz, K. Kuramochi, A. Parihar, B. Brahimaj, E. Grotewold and A. I. Doseff, Molecular basis for the action of a dietary flavonoid revealed by the comprehensive identification of apigenin human targets, *Proc. Natl. Acad. Sci. U. S. A.*, 2013, **110**, E2153–E2162.

34 M. Willenborg, U. Panten and I. Rustenbeck, Triggering and amplification of insulin secretion by dimethyl alpha-ketoglutarate, a membrane permeable alpha-ketoglutarate analogue, *Eur. J. Pharmacol.*, 2009, **607**, 41–46.

35 D. R. Sharma, A. Sunkaria, W. Y. Wani, R. K. Sharma, R. J. Kandimalla, A. Bal and K. D. Gill, Aluminium induced oxidative stress results in decreased mitochondrial biogenesis *via* modulation of PGC-1α expression, *Toxicol. Appl. Pharmacol.*, 2013, **273**, 365–380.

36 R. J. Mailloux, J. Lemire and V. D. Appanna, Hepatic response to aluminum toxicity: dyslipidemia and liver diseases, *Exp. Cell Res.*, 2011, **317**, 2231–2238.

37 W. Yue, Z. Chen, H. Liu, C. Yan, M. Chen, D. Feng, C. Yan, H. Wu, L. Du, Y. Wang, J. Liu, X. Huang, L. Xia, L. Liu, X. Wang, H. Jin, J. Wang, Z. Song, X. Hao and Q. Chen, A small natural molecule promotes mitochondrial fusion through inhibition of the deubiquitinase USP30, *Cell Res.*, 2014, **24**, 482–496.

38 S. Lee, F. H. Sterky, A. Mourier, M. Terzioglu, S. Cullheim, L. Olson and N. G. Larsson, Mitofusin 2 is necessary for striatal axonal projections of midbrain dopamine neurons, *Hum. Mol. Genet.*, 2012, **21**, 4827–4835.